QRB QUARTERLY REVIEWS OF BIOPHYSICS
journals.cambridge.org/qrb

REVIEW

Understanding membrane-active antimicrobial peptides

Huey W. Huang* and Nicholas E. Charron

Department of Physics and Astronomy, Rice University, Houston, Texas 77005, USA

Quarterly Reviews of Biophysics (2017), **50**, e10, page 1 of 17 doi:10.1017/S0033583517000087

Abstract. Bacterial membranes represent an attractive target for the design of new antibiotics to combat widespread bacterial resistance to traditional inhibitor-based antibiotics. Understanding how antimicrobial peptides (AMPs) and other membrane-active agents attack membranes could facilitate the design of new, effective antimicrobials. AMPs, which are small, gene-encoded host defense proteins, offer a promising basis for the study of membrane-active antimicrobial agents. These peptides are cationic and amphipathic, spontaneously binding to bacterial membranes and inducing transmembrane permeability to small molecules. Yet there are often confusions surrounding the details of the molecular mechanisms of AMPs. Following the doctrine of structure–function relationship, AMPs are often viewed as the molecular scaffolding of pores in membranes. Instead we believe that the full mechanism of AMPs is understandable if we consider the interactions of AMPs with the whole membrane domain, where interactions induce structural transformations of the entire membrane, rather than forming localized molecular structures. We believe that it is necessary to consider the entire soft matter peptide-membrane system as it evolves through several distinct states. Accordingly, we have developed experimental techniques to investigate the state and structure of the membrane as a function of the bound peptide to lipid ratio, exactly as AMPs in solution progressively bind to the membrane and induce structural changes to the entire system. The results from these studies suggest that global interactions of AMPs with the membrane domain are of fundamental importance to understanding the antimicrobial mechanisms of AMPs.

* Author for correspondence: H. W. Huang, Department of Physics and Astronomy, Rice University, P. O. Box 1892, Houston, TX 77251, USA. Tel: 713 348 4899; Email: hwhuang@rice.edu

1. Introduction

Prior to the discovery of antimicrobial peptides (AMPs), most research efforts on membrane-active agents focused on elucidating discrete ion channel conductance observed in black lipid membrane (BLM) experiments. Initially, the interest on membrane-active compounds was due to their ability to create single channel electric excitability in a BLM. Such compounds were called excitability-inducing materials (EIMs) (Latorre & Alvarez, 1981; Mueller & Rudin, 1968). Most of EIMs were isolated from cultures of microorganisms and many of them were antibiotics. At the time there was a great deal of interest in excitable membranes but no channel structure had yet been isolated or characterized biochemically. Investigators were looking for molecular mechanisms of channel opening and closing that could shed light on similar processes in excitable cell membranes. Because of the low background conductance of a BLM (typically 10 pS for 1 mm^2 of membrane), it is possible to measure channel conductance in the order of 1 pS induced by EIMs.

Discrete single channel electrical conductance, displayed by a series of randomly fluctuating open and closed states, was typically observed in a BLM exposed to an EIM concentration in the nanomolar range (Latorre & Alvarez, 1981). These channel activities were explained by a barrel-stave model, namely a pore in the membrane composed of a bundle of EIM molecules inserted in the membrane (Baumann & Mueller, 1974; Latorre & Alvarez, 1981). This was particularly successful for alamethicin, whose crystal structure was determined by X-ray diffraction (Fox & Richards, 1982). The barrel-stave model could indeed account for the details of single channel kinetic behavior induced by alamethicin (Mak & Webb, 1995). However, alamethicin turned out to be a rather special case.

Host-defense AMPs from animals were first discovered in insects in the early 1980s, and subsequently found in almost every organism (Boman & Hultmark, 1987; Boman *et al.* 1994; Steiner *et al.* 1988; Wade *et al.* 1990; Zasloff, 1987). Initially the discoverers and pioneers of the field wrestled with the questions about the molecular targets of these antibiotics (Boman & Hultmark, 1987; Boman *et al.* 1994; Steiner *et al.* 1988; Wade *et al.* 1990; Zasloff, 1987). By the late 1980s, accumulated evidence, especially the experimental result showing that the natural all-L peptides and their D enantiomers were equally active (Wade *et al.* 1990), convincingly concluded that the main targets of AMPs were the bacterial cytoplasmic membranes, rather than stereospecific molecular receptors (Boman *et al.* 1994). Yet, experiments designed to investigate potential discrete ion channel conductance from AMPs led to atypical results; most natural AMPs are much more electrically charged than the exceptional case of alamethicin, and their resulting ion conductivities were unlike that of alamethicin (Christensen *et al.* 1988). Since then a major question on the AMPs concerns the details of their molecular mechanisms acting on the bacterial cytoplasmic membranes. While studies with live bacteria have been carried out (Barns & Weisshaar, 2013; Fantner *et al.* 2010; Rangarajan *et al.* 2013; Sochacki *et al.* 2011; Steiner *et al.* 1988), they are complicated by both the presence of outer membranes and the fact that the action of antimicrobials could induce secondary effects including activation of autodigestive enzymes resulting in cell membrane lysis (Bierbaum & Sahl, 1987; Elsbach & Weiss, 1993). Thus how AMPs actually kill microbes is more or less an open question (Zasloff, 2002), although permeabilization of membranes should be sufficient to kill a cell.

A second major reason for believing that AMPs target the membranes rather than specific molecular receptors is that the effects of AMPs on lipid vesicles were strongly correlated with their effects on bacteria (Steiner *et al.* 1988). Since the 1980s it was believed that the primary action of AMPs is compromising the permeability of bacterial membranes (Merrifield *et al.* 1994b). Thus biophysical studies on AMPs have been performed primarily with model membranes or lipid bilayers. Essentially this is a particular form of material research, i.e. studying the material property of lipid bilayers in the presence of antimicrobials. Not surprisingly, almost all the known spectroscopies and techniques in material research have been applied to these studies. However there is no standard way of relating the material properties to the mechanism of an antimicrobial and no single measurement is able to fully characterize the interaction of AMPs with membranes. As such, there have been many different interpretations based on as many different measurements. Additionally, the lack of correlations between several different types of experiments results in often incomplete descriptions of a mechanism. A common clause in the literature of AMPs is 'but the mechanism is still unknown.' Yet there is no consensus as to what constitutes a mechanism. This is perhaps the most confusing issue in the field.

Another cause of confusion is due to the strong concentration dependence of AMP behavior in membranes. Phenomenologically, in the range of nanomolar concentrations, AMPs induce transient events of ion conduction in a membrane, but no leakage of glucose or larger molecules (Christensen *et al.* 1988; Duclohier *et al.* 1989; Merrifield *et al.* 1994a).

https://doi.org/10.1017/S0033583517000087

With the exception of alamethicin (Gordon & Haydon, 1972; Mak & Webb, 1995), AMPs produced irregular transient ion conductance that yielded little information about the molecular actions (Boman *et al.* 1994; Christensen *et al.* 1988). At concentrations higher than 100 micromolar, these molecules act as surfactants or detergents that disintegrate lipid bilayers (Nomura *et al.* 2001; Urbaneja *et al.* 1988). The biological activities of AMPs are typically measured in the micromolar range. Indeed, the measured minimal inhibitory concentrations (MICs) are all in this range (Boman *et al.* 1994). Therefore the appropriate range of solution concentration for the study of antimicrobial mechanisms must be in micromolar range.

We believe that a common view follows the structure–function relationship doctrine regarding AMPs as membrane pore-formers. In this spirit, one emphasizes the local peptide–lipid interactions as the mechanism. However, we have taken a different view. While the local peptide–lipid interactions partially explain the resulting peptide-lipid structures, it is the collective peptide–lipid interactions over the whole membrane domain that transform the membrane structure; there are global effects on the membrane domain induced by AMPs that play key roles in the formation of pores and the resulting molecular leakage.

Conventional antibiotics are known to target specific protein receptors in bacteria, interrupting metabolic reactions and cell growth. In contrast to such microbistatic effects, the gene-encoded self-defense AMPs do not have specific protein targets. Instead, they permeabilize the lipid matrix of cell membranes and kill cells (Boman *et al.* 1994). Well-known examples of these microbicidal peptides are cecropins from insects, magainins from amphibians, and defensins from mammals etc. Their mechanisms of permeabilizing the bacterial membranes have been controversial, since molecular events in the target membrane are often difficult to discern due to timescale and spatial resolution limits. Nevertheless, in view of the alarming rise of bacterial resistance to the conventional antibiotics, there are strong incentives to bring non-conventional antimicrobial agents into clinical use. This calls for a deeper understanding of the membrane-acting mechanisms. A well understood membrane permeabilization mechanism is also potentially utilizable for drug and gene delivery.

Our research on membrane-active peptides started with two unique channel formers, gramicidin (Huang, 1986; Olah *et al.* 1991) and alamethicin (Huang & Wu, 1991; Wu *et al.* 1990), using X-ray diffraction and oriented circular dichroism. Once we started our research on antimicrobial peptides magainin (Ludtke *et al.* 1994, 1995, 1996), protegrin (Heller *et al.* 1998, 2000) and others, we were struck by the similarity exhibited by different AMPs from diverse sources in their interactions with membranes. Pore formation in membranes seems to be a natural consequence of the cationic/amphipathic molecular structures of AMPs, as evidenced by X-ray and neutron diffraction experiments; commonly studied peptides such as melittin, LL37, and alamethicin all exhibited characteristic pore-forming behaviors in lipid membranes. However this view was overturned by the experimental results of penetratin. Despite having a cationic/amphipathic molecular structure similar to magainin, LL37, and melittin, penetratin does not induce membrane pores. Furthermore, the FDA-approved antibiotics daptomycin, a cyclic lipopeptide, and anti-fungal amphotericin B, a polyene macrolide, both kill target cells by membrane permeabilization to atomic ions, but they do not form pores for leakage of molecules. The mechanisms of daptomycin and amphotericin B remain unknown despite years of clinical usage, research, and demonstrated membrane affinity. This review will primarily focus on the techniques and results of AMP research with the bigger picture of membrane-active molecules in mind. While the characteristics of AMP-membrane systems may not be representative of all membrane-active peptides and macrolides, we believe there is a distinct benefit in approaching the study of these other agents in the same soft matter systemic fashion.

Over two decades, we have developed various methods for extracting structural information from peptide-lipid systems. All data and conceptual ideas that will be mentioned here have been published, but they have not been discussed together from a coherent view. The review starts with a recent close comparison between *Escherichia coli* spheroplast membranes and lipid membranes that suggested no major differences in their reactions to AMPs. We believe that this result justifies the use of lipid membranes for the studies of AMP molecular mechanisms. To mimic the attack of AMPs on bacteria we observed a giant unilamellar vesicle (GUV) in a solution containing AMPs. We then correlate the phenomena observed in GUVs to nano-scale structural data obtained from peptide-lipid mixtures prepared in multilamellar forms. Phenomenologically, the complete mechanism of AMPs appears to involve an evolution of the peptide-membrane system through different structural states. We discuss the thermodynamic basis for such structural transformations, which we believe give further motivation for studying membrane-active antimicrobials in this fashion.

Finally, a supplemental information provides comments on sample preparation and experimental procedures for the studies that have been done in support of this paper. We feel that it is important to reiterate and demonstrate the importance of sample preparation and quality, as well as some not commonly discussed aspects of these commonly used methods. We focus primarily on the techniques related to multilayer samples, as structure/state determination of a soft matter peptide-membrane system is susceptible to several subtle but important pitfalls.

https://doi.org/10.1017/S0033583517000087

2. Comparison of the action of AMPs on *E. coli* spheroplasts and lipid bilayers

The collective review of our AMP research begins by inspecting the interaction of AMPs with bacteria. The action of dye-labeled AMPs on live bacteria has been observed with fluorescence microscopy, showing permeabilization of the cytoplasmic membranes, allowing the AMPs to enter the cell (Barns & Weisshaar, 2013; Fantner *et al.* 2010; Pogliano *et al.* 2012; Rangarajan *et al.* 2013; Sochacki *et al.* 2011; Steiner *et al.* 1988). But the permeabilization was neither characterized nor quantified.

Our approach is to compare the actions of AMPs in bacterial and lipid membranes as closely as possible, to detect the similarities and dissimilarities between the two types of membranes. We can then decide if it is meaningful to use the model membranes to reproduce the action on bacterial membranes. To focus on the interactions of AMPs with bacterial membranes, we used *E. coli* spheroplasts, the cells from which the outer membranes have been removed. The spheroplasts can be stabilized in a STOP solution (Sun *et al.* 2014) in which they exhibit no cell division, but they can revert to the normal form of *E. coli* when returned to a growth medium (Ruthe & Adler, 1985). Before we studied the effect of AMPs, we investigated the physical properties of the spheroplast membranes by the micropipette aspiration method (Sun *et al.* 2014). We found that the properties of the bacterial cell membranes are best described as lipid bilayers with membrane reservoirs, such as membrane folds (Sun *et al.* 2014). The spheroplast membranes are without a surface tension, unless the spheroplast is swollen to its limit (Sun *et al.* 2014). Nonetheless, if a spheroplast is subject to an aspiration pressure, a surface tension will develop reversibly with the applied suction pressure (Sun *et al.* 2014). This tension arises from unfolding and refolding of the membrane reservoir, rather than stretching the lipid bilayer; the apparent area-stretching elastic constant is of order of magnitude smaller than that of stretching a lipid bilayer.

To study the effect of AMPs, spheroplasts were kept in a solution containing dye molecule calcien and LL37, melittin, or alamethicin. The results are shown in Fig. 1 (Faust *et al.* 2017; Sun *et al.* 2016). Under a well-defined condition, the response seen in Fig. 1 is highly reproducible. No calcein leakage into the spheroplast was observed during the initial 5 min control period before the introduction of AMPs. After melittin was added, no leakage was observed for approximately 15 min. Calcein then leaked into the spheroplast and the intracellular fluorescence intensity sigmoidally rose to a steady-state level. The steady-state level of intracellular fluorescence intensity was always less (~0·8 times) than the extracellular intensity level (Sun *et al.* 2016). This rise to steady state was captured using a 60 s interval between image acquisitions, which amounted to very little photobleaching. The interval between acquisitions was then shortened to 5 s and an exponential decay of the intracellular intensity was observed – we call this a photobleaching period. After the photobleaching period, the image acquisition interval was increased back to 60 s and the intracellular fluorescence intensity recovered to the previous steady state. The 5 s photobleaching was repeated at least once during each experiment to make sure that the steady-state levels and exponential decays were internally consistent. When the intracellular fluorescence intensity reached a steady state, the influx and outflux are constant. We employed a method of balancing the transmembrane fluxes with photobleaching (Faust *et al.* 2017; Sun *et al.* 2016) to monitor the instantaneous membrane permeability to a dye molecule, defined by the flux rate j_c (see online S.2 Method 6.2).

We then performed the same experiment with GUVs (Fig. 1). Given the differences between spheroplast membranes and model lipid bilayers in their mechanical properties as measured by aspiration experiments (Sun *et al.* 2014), one might expect different responses to the attack of AMPs. Surprisingly, what occurred in GUVs is very similar to what occurred in spheroplasts (Fig. 1). Firstly, AMPs induced an intra-vesicular fluorescence intensity pattern very similar to that induced in spheroplasts. Secondly, the steady-state permeabilities per unit area induced in spheroplasts and GUVs are in good agreement despite the size variations (Faust *et al.* 2017).

We then compared the action of AMPs with metabolic inhibitor carbonyl cyanide *m*-chlorophenylhydrazone (CCCP), and daptomycin, which causes cell death by inducing membrane permeability to atomic ions. The patterns of leakage induced by CCCP or daptomycin are irregular, very different from the action by AMPs.

We concluded that there are understandable differences between spheroplasts and GUVs, chiefly due to the membrane tension often present in GUVs whereas the spheroplasts maintain a tensionless condition. But the comparisons strongly support the validity of model membranes studies with AMPs. Although there are some aspects of spheroplast experiment that are probably difficult to reproduce by GUVs, ultimately it is clear that experiments with live cells are more limited than those with lipid bilayers. Thus, we rely on model membrane studies to understand the molecular interactions.

https://doi.org/10.1017/S0033583517000087

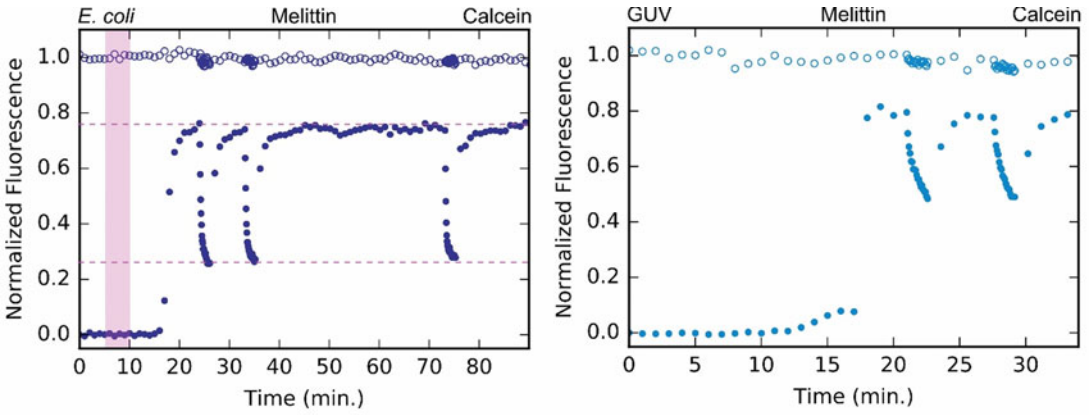

Fig.1. Membrane permeability induced by melittin in *E. coli* spheroplasts and GUV. A confocal time series of an immobilized *E. coli* spheroplasts (left) and a GUV (right) in a perfusion chamber were collected. Solution containing calcein, but no melittin was perfused from 0 to 5 min. followed by perfusion of calcein with 1 μM melittin from 5 to 10 min (shaded pink region, left). Normalized extracellular (open circles) and intracellular (filled circles) calcein fluorescence intensities are shown. The interval between scans was 60 s, until the photobleaching periods where the interval was 5 s. The upper, pink, dashed line (left) is the steady-state level of intracellular fluorescence intensity with negligible photobleaching when the scan interval was 60 s. The lower, pink, dashed line is the steady-state level of intracellular fluorescence intensity during photobleaching when the scan interval was 5 s. This reproducible fluorescence intensity pattern is remarkably similar in spheroplasts and in GUVs (right). Furthermore, the steady-state membrane permeability values measured in spheroplasts and GUVs are the same (Faust *et al.* 2017).

3. Mechanistic studies in lipid membranes

We use a GUV to mimic the attack of AMPs on bacteria. We then correlate the GUV experiment to high resolution measurements performed in multilamellar lipid bilayers. In the following experiments we use melittin as an example of AMPs. The same experiments have been performed with many other AMPs with similar results (see online Supplemental S2).

3.1 Interaction with a GUV

Many investigators have observed molecular leakage through GUVs membranes when AMPs were introduced into the solution (Fuertes *et al.* 2010; Lee *et al.* 2008; Tamba & Yamazaki, 2005). A crucial missing piece of information in such experiments is the bound peptide concentration on the membrane when the leakage occurs. So the question is how to correlate the leakage to a molecular mechanism? Our method is to measure the membrane area change during the GUV experiment. In all membrane-active peptide experiments we have performed, there was always a membrane area expansion as peptides bound to the membrane, as quantitatively measured by micropipette aspiration. What was unexpected was that when we repeated the experiment many times, we discovered a well-defined average fractional membrane area expansion coinciding with the occurrence of molecular leakage. Figure 2 shows an example of such measurements.

In these experiments, which were repeated at least 10 times with different vesicles (Lee *et al.* 2013), the value of the fractional membrane area increase $\Delta A/A$ when the leakage began was measured to be 3·42 ± 0·59%. Note that this numerical value is specific to the lipid composition of the GUV, DOPC/DOPG 7:3 and the peptide melittin (Lee *et al.* 2013).

3.2 Peptide-lipid mixtures in oriented multilayers

One sample type that has produced high resolution structural information for peptide-membrane systems is oriented multilayers, i.e. a stack of parallel bilayers of peptide-lipid mixtures intercalated by water layers of controllable thickness. In such a sample, the majority of the bilayers are free of the influence of the supporting substrate, and the amount of the sample is not limited. However, it is important to be able to ascertain the sample's homogeneity and the uniformity of the multilayers' alignment. The alignment is most conveniently measured by X-ray diffraction (see online S.2 Methods).

There are lyophilization procedures by which peptides, lipids and other components, such as ions, can be homogeneously mixed in a dry powder form, and then hydrated into oriented parallel bilayers. Alternatively, depending on the added components, one may use evaporative deposition of dissolved and mixed lipids and components on a substrate, though this often requires some trial and error (online S.1 Sample preparation). The degree of hydration for a multilayer sample is controllable by the ambient relative humidity (RH), which effectively changes the average thickness of water layers between bilayers. Multilamellar samples can be purposefully overhydrated [e.g. (Lee *et al.* 2011)]. In overhydrated multilayers, bilayers exhibit

https://doi.org/10.1017/S0033583517000087

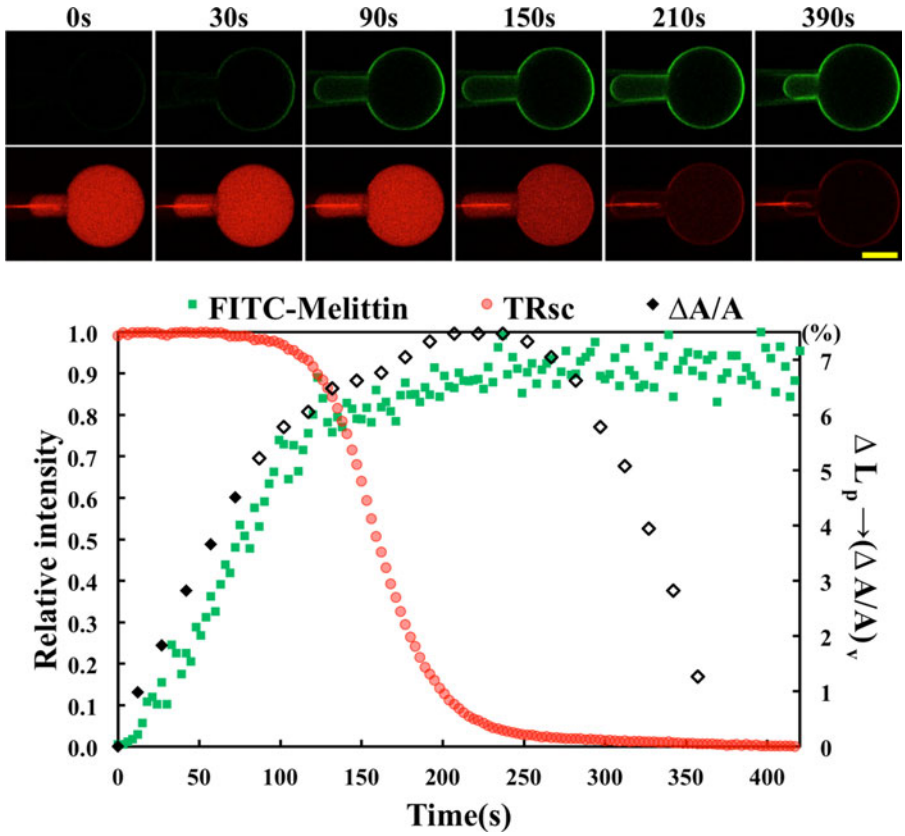

Fig. 2. A run of the GUV experiment (see online Movie S1 in Supplemental). (Upper) Confocal images of an aspirated GUV, in green color to measure the binding of FITC-melittin on the GUV and in red color to measure the fluorescence intensity of TRsc (MW 625) inside the GUV. A GUV of DOPC/DOPG 7:3 composition encapsulating TRsc was introduced into a solution containing 2 μM FITC-melittin at time zero. Within ~400 s, photobleaching of the dyes was negligible. Scale bar = 20 μm. (The red line on the micropipette is an optical artifact.) (Lower) The fractional GUV area change $\Delta A/A$ (solid and empty diamonds, calculated from the protrusion length change ΔL_p inside the micropipette, scale on the right ordinate) and relative fluorescence intensities in time (scale on the left ordinate): green squares for the FITC-melittin on the GUV surface; red circles for the dye TRsc inside the GUV. The strongest fluorescence intensity for each color is taken as 1. (Lee *et al.* 2013).

thermal undulations similar to a free bilayer (Lee *et al.* 2011; Safinya *et al.* 1989; Wack & Webb, 1989). At the condition equilibrated by ~100% RH, the thermal undulations of individual bilayers are dampened. In this condition, the physical state of the peptide-lipid mixture is close to a free membrane and can be precisely measured by diffraction and other methods.

To correlate with the GUV membrane immersed in a solution containing AMPs, we imagine that the state of membrane continuously changes with an increasing number of bound peptides. The same lipid composition used in the GUV experiment, i.e. DOPC/DOPG 7:3, was mixed with melittin in a series of peptide-to-lipid molar ratios, *P*/*L*, and prepared in the multilamellar form, in order to emulate the evolution of the GUV experiment at specific points in time from the initial exposure to the onset of leakage.

3.2.1 X-ray diffraction and oriented circular dichroism

X-ray lamellar diffraction serves two purposes. The first is to examine the quality of the multilayer sample. By rotating the plane of substrate against the incident X-ray beam (which produces the rocking curve), one examines the alignment of the multiple layers. By measuring the multilayer repeat distance D *versus* RH, one can determine if the sample is close to the full hydration (Weiss *et al.* 2003). Without this crucial examination of sample quality, the subsequent measurement from the sample could produce very misleading results. For instance, if the multilayers are not well aligned, the peptide orientation will not be uniform and any subsequent peptide orientation measurement will be averaged out through the sample. Specifically oriented circular dichroism measurements rely on the uniform layer alignment throughout the sample.

The second purpose of X-ray diffraction is to reconstruct the electron density profiles of the bilayers. From the precisely measured phosphate-to-phosphate distance, *PtP*, across the bilayer (Fig. 3), we obtained the thickness of the hydrocarbon region *h*

https://doi.org/10.1017/S0033583517000087

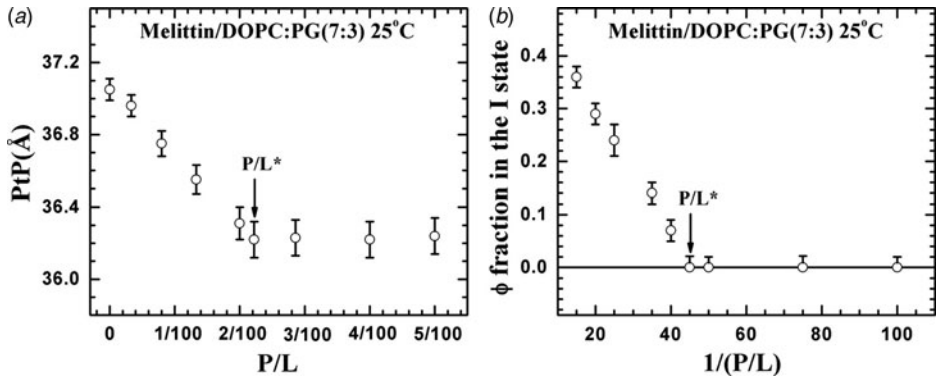

Fig. 3. Melittin and lipid (DOPC/PG 7:3) mixtures in a series of molar ratio P/L, in fully hydrated multilayers. (*a*) The membrane thickness, PtP, as a function of P/L measured by X-ray lamellar diffraction. PtP linearly decreases with P/L until $P/L^* \sim 1/45$. (*b*) The same samples were measured by the method of OCD to determine the fraction of melittin helices oriented normal to the plane of bilayers (the remaining fraction were parallel to the plane). The fraction is linear when plotted against $1/(P/L)$ (Lee *et al.* 2004) for P/L above a transition point $P/L^* \sim 1/45$. The error bars are that of reproducibility using two to three independently prepared samples (Lee *et al.* 2013).

(online S2. Methods). In the case of melittin in DOPC/PG 7:3, the membrane thickness initially decreased linearly with the peptide-to-lipid molar ratio P/L, but above a critical value $P/L^* \sim 1/45$, the membrane thickness leveled off. The fractional membrane thinning was $-\Delta h/h = 3.3 \pm 0.2\%$ at $P/L = P/L^*$.

The same samples were also measured by oriented circular dichroism (OCD) (Wu *et al.* 1990; Yang *et al.* 2001) to characterize the orientation of melittin helices in membranes (Fig. 3). All melittin helices were found to lie parallel to the plane of membrane in the region the thickness decreased linearly with P/L; but above the critical $P/L^* \sim 1/45$ an increasing fraction of melittin helices changed orientation to perpendicular to the membrane (Fig. 3). This correlation between the membrane thinning and the peptide orientation change has been observed for melittin and other antimicrobial peptides in many different lipid compositions (Huang, 2000; Lee *et al.* 2004, 2005). Only the value of P/L^* and the degree of thinning varied with peptide and lipid composition.

Both X-ray lamellar diffraction and OCD provide valuable information about the state of peptides in the membrane, as well as their important effects on the bulk of the multilayer system. By investigating the multilayer samples in varying peptide to lipid ratios, the evolution of the entire soft matter system can be investigated. Furthermore, the orientation states of peptides in the multilayer may be directly correlated with hydrocarbon thickness modulations, suggesting that physical changes in the peptides results in a global effect on the sample. This is precisely why we believe that a full understanding of AMP mechanisms originates from considering the global state changes of a soft matter peptide-membrane system.

3.2.2 Neutron in-plane scattering

The GUV experiments show that molecular leakage occurs at a certain peptide-to-lipid ratio. On the other hand, X-ray lamellar diffraction and OCD show that a critical peptide concentration marks a global transition of the peptide-membrane system, i.e. a structural and peptide orientation changes occur at the peptide-to-lipid ratio P/L^* in multilamellars. These two observations suggest that leakage is correlated with a specific global structural transition. One explanation for structurally induced molecular leakage is the formation of pores. If pores are present in the bilayers, there is an easy way to detect them by neutron in-plane scattering off oriented multiple bilayers (He *et al.* 1995, 1996; Ludtke *et al.* 1996). The water through the pores can be replaced with D_2O, simply by replacing the hydrating H_2O vapor with D_2O vapor. Viewed along the plane of the bilayer, the D_2O columns through the pores will stand out in high contrast against the lipid background for neutron scattering, due to the very high deuterium–neutron scattering length (Fig. 4).

We have tested at least five different peptides in various compositions of lipids (online Supplemental S2). We found that pores were present when P/L was above P/L^* but not when it was below (He *et al.* 1995; Lee *et al.* 2011; Ludtke *et al.* 1996; Yang *et al.* 1998, 2001). Neutron results show that the density and size of pores in multilayers are constant in time. A GUV with stable pores can last for an hour or longer, apparently in an equilibrium state (Last & Miranker, 2013; Lee *et al.* 2008). Therefore, we conclude that pores formed by peptides in ratios above P/L^* are stable membrane structures.

The density of the pores in the membrane and the fraction of melittin oriented normal to the plane of bilayers (as measured by OCD) suggested that there are 4–7 melittin helices in the luminal surface of a fully hydrated pore (Ludtke *et al.* 1996; Yang

https://doi.org/10.1017/S0033583517000087

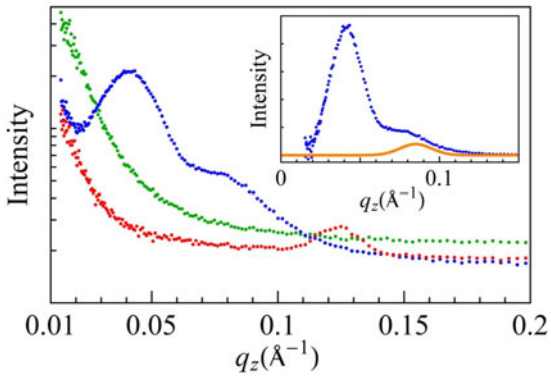

Fig. 4. Neutron in-plane scattering of LL37 in DOPC at $P/L = 1/50$ in three conditions: red–equilibrated at 100%RH D_2O; blue–equilibrated with excessive D_2O in an overhydrated state; green – equilibrated with excessive H_2O in an overhydrated state. Inset: Reduced data obtained from the blue curve after removing the background (the empty sample cell). The shoulder peak was fit with a Gaussian curve (orange) at 0·085 Å^{-1} corresponding to a D spacing of 74 Å in the overhydrated state. The broad peak at 0·041 Å^{-1} is due to the presence of D_2O columns in the membrane, implying the presence of transmembrane pores. The sample was a LL37/lipid mixture prepared in a multilamellar form. We found that LL37 oriented parallel to the bilayers in all hydrations up to 100% RH (perhaps due to its length). Only in the overhydrated condition (i.e. with thick water layers), LL37 turned into the perpendicular orientation (Lee *et al.* 2011).

et al. 2001). The molecular cross section of a melittin helix along its axis has been measured to be 4·00 nm^2 (DeGrado *et al.* 1981; Terwilliger *et al.* 1982). The total area contributed by a maximum of 7 melittin helices to the luminal surface is ~28 nm^2 (Yang *et al.* 2001) out of a total area of $4.4\pi \times 3.7 \sim 51$ nm^2 (assuming a bilayer height 3·7 nm based on the PtP in Fig. 3). Thus 50% or more of the luminal surface is lined by the lipid headgroups.

3.3 Correlation of leakage in GUVs with pores detected in multilayers

By comparing the results of X-ray and OCD studies in multilamellar samples with the microscopy studies of GUVs, a close correlation can be found between the state of membrane in the GUV before dye leakage and the state of membrane in multilayers before pore formation. Again, we examine the representative case of melittin: In a GUV, the membrane area expansion is linearly proportional to the fluorescence intensity due to the binding of dye-labelled melittin (Fig. 2); in multilayers, the membrane thinning is linearly proportional to P/L (Fig. 3). The fractional membrane area expansion reached $\Delta A/A = 3.4 \pm 0.5\%$ when dye leakage began (Fig. 2); the fractional membrane thickness decrease was $-\Delta h/h = 3.3 \pm 0.2\%$ when stable pores began to appear in the multilayers Fig. 3. This close correlation reasonably suggests that the state of membrane in the GUV and the state of membrane in the multilayers was the same before the formation of stable pores. Furthermore, noting that multilayer samples are prepared with peptides evenly distributed on both sides of lipid bilayers, it suggests that melittin monomers initially bound to the outer leaflet of GUV had redistributed to both sides of the membrane before the formation of stable pores in the GUV.

The equality of $\Delta A/A$ and $-\Delta h/h$ comes from the volume conservation of the hydrocarbon region (area A times thickness h), assuming that melittin binding has insignificant penetration into the hydrocarbon region (Terwilliger *et al.* 1982). The samples studied by X-ray were also measured by OCD (Wu *et al.* 1990; Yang *et al.* 2001) for the orientation of melittin helices in membranes (Fig. 3). The results showed that the α-helical peptides bound parallel to the plane of the bilayer before the pore formation when $P/L < P/L^*$. It is under this condition, the equality of $\Delta A/A$ and $-\Delta h/h$ applies ($A \cdot h$ = constant. $\Delta(A \cdot h) = 0$ implys $\Delta A/A = -\Delta h/h$). As the pores began to appear, a fraction of peptides also turned to the perpendicular orientation, and this fraction increased as P/L increased above P/L^*. The equality of $\Delta A/A$ and $-\Delta h/h$ is not applicable when $P/L > P/L^*$.

3.4 The structure of AMP-induced pores

It is perhaps debatable based on the GUV experiment alone whether stable pores are formed by AMPs in membranes. There is no way of ascertaining the molecular structures or events responsible for membrane permeabilization using GUV experiments alone. These experiments may only indicate the presence of molecular leakage as well as ceratin bulk structural changes such as tension or area changes. More direct evidence is absolutely necessary to establish the existence of pores, let alone determining their structures. Fortunately, multilayer samples allow for the extraction of equilibrium structures that depend on peptide concentrations. The existence of pores was provided by neutron scattering in fully-hydrated multilayers of lipid-peptide mixtures (Ludtke *et al.* 1996; Yang *et al.* 2001). The detected pores were in a two-dimensional fluid of lipid bilayer (Ludtke *et al.* 1996; Yang *et al.* 2001). The radial distribution function deduced from the scattering curve had a narrow peak indicating

https://doi.org/10.1017/S0033583517000087

a uniform pore size (Ludtke *et al.* 1996; Yang *et al.* 1999, 2001). The inner diameter of the melittin pore was found to be ∼4·4 nm in either POPC (at $P/L = 1/15$) or DLPC (at $P/L = 1/30$) bilayers (Yang *et al.* 2001). As discussed in Yang *et al.* (2001), these pores could not be formed by barrel-like assemblies of peptide helices (the so-called barrel stave model) (Baumann & Mueller, 1974; Qian *et al.* 2008a)) because the fraction of melittin helices measured to be oriented perpendicularly to the membrane was much less than what was required to line the inner circumferences of all the pores (in contrast, this was possible for alamethicin, which forms barrel-stave pores (He *et al.* 1996)). Therefore, it was argued that the pore must be at least partially lined by the lipid headgroups. This resulted in the development of the toroidal (or wormhole) pore concept (Ludtke *et al.* 1996). A defining topological difference exists between the barrel-stave and toroidal pores: in the former, the inner pore surface is completely lined with closely-packed peptides that punch directly through the length of the membrane such that the surface formed by the headgroups is discontinuous in the pore vicinity. In the latter, the partial lining of the inner pore surface results in a local bending of the lipids such that the surface formed by the headgroups is continuous through the inner surface of the pore. About the same time the same model was proposed by Matsuzaki *et al.* (1996, 1997) based on their kinetic experiments.

Surprisingly it is possible to crystalize pores in multilayers (Yang *et al.* 2000). Upon dehydration, multilayers with pores as detected by neutron in-plane scattering transformed from the lamellar phase to a rhombohedral (R) phase (Fig. 5) (Lee *et al.* 2013; Yang *et al.* 2000). In such a softmatter crystalline, the unit cell is composed of a liquid-like distribution of lipids and peptides. As a result, the diffraction is limited to small angles (Qian *et al.* 2008a, b), even though the diffraction peaks are sharp (implying an excellent long-range order). To make use of such low-resolution diffraction, we simplified the detected component to highlight only the contour of the pore. This was accomplished by using a Br-labeled lipid, di18:0(9,10Br) PC, and developing a method of multiwavelength anomalous diffraction (MAD) to obtain the diffraction amplitudes for the Br atoms alone (online S2. Methods). (A note on the lipid di18:0(9,10Br)PC: melittin has been studied in a great variety of lipid compositions; the behavior of stable-pore formation is similar in all, including the phase transition from the lamellar phase to the R phase (Lee *et al.* 2004, 2005, 2008; Yang *et al.* 2001); there is nothing special about di18:0(9,10Br)PC). Figure 6 shows the distribution of Br atoms in a unit cell in which the top and bottom monolayers bend and merge through the pore, confirming the topological signature of the toroidal model (Lee *et al.* 2013).

The purpose of the crystal reconstruction is to provide the structural proof that the melittin pore is lined by the bilayer interface. In fully hydrated multilayers, neutron scattering determined the internal diameter of the melittin pores to be 4·4 nm (Yang *et al.* 2001). Upon dehydration to the R phase, the inner diameter of the melittin pore was reduced to ∼0·7 nm. The same results were found in pores induced by other AMP peptides (Qian *et al.* 2008b). Reconstructions of barrel-stave pores formed by alamethicin can also be recovered in this fashion (Qian *et al.* 2008a).

4. The free energy pathway

We now propose a conceptual framework for understanding the experimental observations described above. Before we do so, we note that most AMPs under consideration are ∼20–40 amino acid long and they are most likely too small to have a single molecular function in a membrane. Also the molecular properties of AMPs are probably not designed to form multi-molecular complexes, since the majority of known AMPs are strongly cationic, e.g. 11 of 37 amino acids of LL37 are either lysine or arginine; strong electrical repulsion is not favorable for multi-peptide complexing or oligomerization. Alamethicin, an electrically-neutral amphipathic molecule, is an exception (Mak & Webb, 1995). (We note that magainin can polymerize into filaments, but only at high ionic concentrations (Urrutia *et al.* 1989).)

4.1 Evolution of a lipid bilayer in a peptide solution

4.1.1 Initial binding of peptides

Motivated by experimental observations of peptides in lipid bilayer systems, a conceptual framework from basic physical principles can be developed. Let us imagine the process of melittin-based pore formation in a GUV as described in Section 3.1. Individual peptides spontaneously bind to the interface of the lipid bilayer due to their molecular amphiphilicity. Melittin has the conformation of a bent α-helical rod with a distinctive orientational segregation of hydrophobic and hydrophobic side chains.(Terwilliger *et al.* 1982). The hydrophobic side chains are oriented mainly towards the inside of the bend of the helix, and the charged and polar side chains are oriented mainly towards the outside of the bend. Thus melittin integrates into the surface of the lipid bilayers with the helical axis parallel to the bilayer (as shown by OCD) in which the hydrophobic inner surface penetrates shallowly in the non-polar portion of the membrane (Terwilliger *et al.* 1982).

https://doi.org/10.1017/S0033583517000087

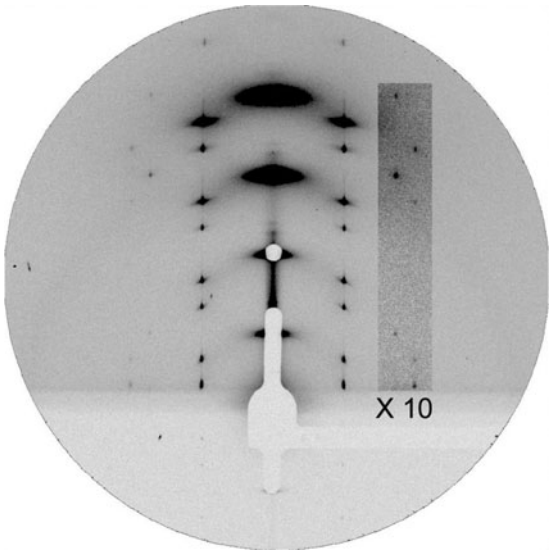

Fig. 5. Grazing angle diffraction pattern of the R phase of a melittin-di18:0(9,10Br)PC mixture with $P/L = 1/40$ at 45% RH, 30 °C (Lee *et al.* 2013).

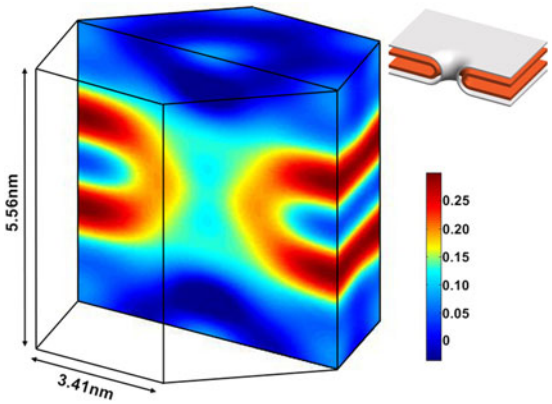

Fig. 6. X-ray contour of the melittin pore in the R phase of a melittin-di18:0(9,10Br)PC mixture ($P/L = 1/40$). To show the contour of the melittin pore clearly, we used the multiwavelength anomalous diffraction method to obtain the diffraction amplitudes for Br atoms alone. The solid lines define the unit cell of the R phase. The electron density is expressed in a relative scale by color. Br atoms are distributed in the high density (yellow-red-black) region. The non-uniformity in the low density region is due to the limited resolution of small angle diffraction. A cartoon for the lipid structure shows the basic topology: the silver layer represents the headgroup layer of the lipid bilayer, and the red layer represents the Br layer, which was detected by X-ray (Lee *et al.* 2013).

The key feature of this interaction is that melittin occupies space in the headgroup region of the phospholipid molecules in the bilayer, but does not extend all the way to the center of the bilayer. In order that there may not be any empty space underneath the melittin molecule, the lipid chains must be distorted from a smooth planar bilayer to fill the space. By contrast, any protein of uniform cross section that naturally penetrates all the way across the bilayer or exactly half-way across the bilayer would not be expected to disturb the bilayer structure in the same manner as melittin. The presence of bound melittin peptides in the headgroup region also results in a membrane area increase, while the lipid chains distortion as described above results in a local thinning of the lipid bilayer.

It has been estimated that the free energy barrier for translocating a single melittin molecule across a lipid bilayer is about 30 k_BT (Lee *et al.* 2013; Moon & Fleming, 2011). Thus it is very unlikely for an individual peptide to translocate by itself from thermal fluctuations alone. However, we have seen that the initial membrane area expansion of the GUV by melittin binding was in agreement with the membrane thinning measured in the multilayers, implying that the melittin must be on both sides of the bilayer of the GUV before pore formation. Indeed it has been observed experimentally that bound peptides rapidly translocated from the outside leaflet to the inside leaflet of the bilayer (Matsuzaki *et al.* 1995).

https://doi.org/10.1017/S0033583517000087

Because thermal fluctuations of individual peptide cannot account for translocation, the most reasonable assumption for melittin translocation before the formation of stable pores is by way of transient pore fluctuations. It was known since the early days of its discovery that melittin (and other antimicrobial peptides) induces transient ion conduction at nanomolar peptide concentrations (Hanke *et al.* 1983; Merrifield *et al.* 1994a; Tosteson & Tosteson, 1981). The ion conductivity increases with the peptide concentration all the way to the sub-micromolar range (Hanke *et al.* 1983; Tosteson & Tosteson, 1981). We define the pores that induce atomic ion conduction but do not allow transmembrane passage of glucose or larger molecules as transient pores. The transient pores induced by melittin (or other AMPs) do not exhibit well-defined single-channel step-conductance, contrary to the exceptional case of alamethicin (Hanke *et al.* 1983; Merrifield *et al.* 1994a). The molecular configurations of transient pores are unknown and may very well be generally non-specific. Given how tightly melittin binds to the interface and the relatively low energy barrier for toroidal pore formation, the transient pore formation is likely due to the stress from one-sided binding that increases the area of the outer leaflet relative to the unperturbed inner leaflet (Terwilliger *et al.* 1982). Thus, transient pores can occur locally by fluctuations as evidenced by transient ion conductions at extremely low peptide concentrations.

Before molecular leakage occurs, the distribution of peptides throughout the bilayer appears to be uniform as measured carefully by fluorescence energy transfer experiments (FRET) (Gazit *et al.* 1994, 1995; Hirsh *et al.* 1996; Schümann *et al.* 1997). This finding is in agreement with a theoretical argument that the interfacial-bound peptides experience mutually repulsive membrane–mediated interactions (Huang, 1995). The peptide binding incurs a positive energy of bilayer deformation, i.e. a local membrane thinning. According to the elasticity theory (Helfrich, 1973), the energy of membrane deformation is proportional to the square of the amplitude of thinning. As a result of this square rule, the energy cost of bilayer deformation would increase if two far separated bound peptides approach each other. The repulsive force between two bound peptides extends over a separation distance of about 25 Å (Huang, 1995). Therefore the peptides bound on the bilayer interface must be monomeric, in agreement with FRET experiment (Schümann *et al.* 1997).

4.1.2 The transition to pore formation

In the region $P/L \gtrsim 1/100$, the membrane thinning by peptide binding is large enough to be measured by X-ray diffraction and the thinning is invariably in linear proportion to P/L, until P/L reaches a critical value P/L^* whose value depends on the peptide as well as the lipid composition. For $P/L > P/L^*$, the membrane thickness remains approximately constant despite increasing number of bound peptides. Coincidentally pores begin to appear in the bilayers as P/L exceeds P/L^* as shown by leakage or neutron scattering. How can we understand this transition as a function of P/L? We believe that a complete quantitative theory is very complicated, but we can at least understand the key aspects of this transition at the qualitative level with some mathematical rigor. This will provide a conceptual framework for understanding the mechanism of AMPs.

Perhaps the simplest argument for the transition to a state of membrane with pores is as follows. Beginning with the initial exposure of the lipid bilayer to peptides, peptide binding continues as long as the binding energy is negative (relative to the peptides in solution). This binding causes membrane thinning but there must be some limit of thinning for a lipid bilayer. Therefore, after the bilayer thinning reaches a limit corresponding to the ratio P/L^*, the bilayer forms pores to create additional binding surface on the walls of the pores.

This explanation, while plausible, leaves much to be desired and has no physical basis. Because the phenomena emergent from AMP interactions with lipid bilayers involves a phase transition of the entire system, statistical mechanics offers the appropriate tools for description. Specifically, we appeal to the Landau free energy expansion, a technique of statistical mechanics that offers a mathematical description of phase transitions. We start with the free energy that describes a pore in a lipid bilayer (Litster, 1975; Taupin *et al.* 1975):

$$F_o = 2\pi R\gamma - \pi R^2\sigma \tag{1}$$

where R is the radius of a circular pore, σ is the membrane tension (which is the energy per unit area) and γ is the line tension (the energy cost for creating a unit length of pore edge). This free energy does not support a stable pore, because the free energy F_o has an unstable maximum at $R = \gamma/\sigma$ as a function of the radius R. This was demonstrated experimentally with a GUV (Brochard-Wyart *et al.* 2000; Karatekin *et al.* 2003; Puech *et al.* 2003), in which a pore could spontaneously open or be induced by perturbation. Its behavior was indeed governed by the Eq. (1). If the radius was smaller than $R^* = \gamma/\sigma$, the pore closed; however, if the radius was larger than $R^* = \gamma/\sigma$, the pore expanded indefinitely until the vesicle lysed, following the path of minimizing the free energy.

If, however, the membrane includes bound peptides, Eq. (1) needs to be modified, because the membrane energy per unit area, σ, is a function of the concentration of bound peptides, due to the membrane thinning effect. At the peptide lipid ratio $P/L < P/L^*$, all peptides are bound on the interface of pore-free bilayer. The fractional change of the membrane area

https://doi.org/10.1017/S0033583517000087

associated with peptide binding is $\Delta A/A = (A_P/A_L)(P/L)$, where A_P is the area increment caused by one bound peptide and A_L the area per lipid. This area expansion creates a stress equivalent to a membrane tension K_a $(\Delta A/A)$, where K_a is the membrane stretching elasticity coefficient. When $P/L > P/L^*$, pore formation occurs and the peptides localized to the inner surface of the pores do not contribute to the membrane thinning. Therefore $\Delta A/A = (A_P/A_L)(P - P_I)/L$ and the corresponding tension is $\sigma = K_a\ (A_P/A_L)(P - P_I)/L$. P_I is the total number of peptides adsorbed to the inner surface of the toroidal pores, which is proportional to the radius of the pores: $P_I = \alpha R$, with a proportionality constant α.

Substituting this expression of σ into Eq. (1), we obtain a free energy for pore formation,

$$F = 2\pi\gamma R - \pi\sigma_o R^2 + \alpha\pi K_a[A_P/(A_L L)]R^3 \tag{2}$$

where $\sigma_o = K_a\ (A_P/A_L)P/L$. This free energy can be viewed as a Landau free energy (Landau & Lifshitz, 1965) with an order parameter R in which the effect of decreasing temperature is replaced by the effect of increasing P/L (Fig. 7). There is a critical value P/L^*, such that for $P/L < P/L^*$, the stable state has $R = 0$, or no pores. But for $P/L > P/L^*$, the minimum free energy state has a non-zero positive R, that results in the physical presence of pores (see details in Huang *et al.* (2004)). The free energy approach to describe the action of AMPs clearly highlights the need to consider an entire soft matter peptide-membrane system. It simultaneously motivates and physically explains the experimental investigations that we have carried out.

Alternatively, the transition from a pore-free membrane to a membrane with pores can be studied by the equality of the chemical potentials of the peptides in two phases: the phase without pores and the phase with pores (Huang, 2009). The essential feature of the chemical potential of peptides before pore formation is a term due to the membrane thinning effect. This term is positive, linearly increasing with P/L. On the other hand, the essential feature of the chemical potential of peptides bound to pores is an aggregation effect of multiple peptides in each pore. Specifically, let the number of peptides in each pore be n, and the fraction of the peptides in pores be X_n and the fraction of the peptides bound on the planar interface be X_1. Then the chemical equilibrium demands that X_n is proportional to X_1^n.

In solution, the proportionality $X_n \propto X_1^n$ describes a micellization effect (Debye, 1949) with a critical micellization concentration (CMC). That is, there are practically no micelles as long as the concentration X_1 is smaller than CMC. It is easy to show that, in solution, micellization is possible only if the number n is sufficiently large, at least 15 (Debye, 1949; Huang, 2009). But this is different in a membrane; pore formation in membrane can occur in a fashion similar to a micellization effect with n as small as 4, based on the chemical potential argument where the intrinsic reason is the membrane thinning effect as discussed above (Huang, 2009). This agrees with the experimental observation that 4–7 melittin helices line the luminal surface of each toroidal pore (Ludtke *et al.* 1996).

4.2 Conclusive remark, a lesson from penetratin

The theoretical arguments described above, mainly Eq. (2), are obviously not specific to a particular peptide; in a sense it describes the behavior of amphiphilic peptides that have a binding affinity to the bilayer interface, where the values of parameters γ, σ_o, α, K_a, A_P, and A_L all depend on the specific lipid and peptide mixture under investigation. However, this theoretical approach takes no other peptide properties into account. There exist some peptides that do not appear to be directly describable by the theoretical concept above. As a specific case, we are presently surprised by a counter-example in a peptide called penetratin, although it is not an AMP. Having developed both an experimental and theoretical framework for studying AMPs, it is instructive to investigate why penetratin is not a pore forming peptide.

Penetratin (RQIKI WFQNR RMKWK K) is a 16-residue peptide corresponding to the third helix of the Antennapedia homeodomian of *Drosophila* (Qian *et al.* 1989). This peptide is cationic, amphiphilic, and water soluble. It was studied as a cell-penetrating peptide but its purported membrane-penetrating mechanism remained controversial (Duchardt *et al.* 2007; Fischer *et al.* 2006; Melikov & Chernomordik, 2005). In water, penetratin is a random coil but it spontaneously binds to membranes and turns into an α helix. All of these properties are very similar to LL37, magainin, or melittin. Given the experimental results and the guiding theoretical framework developed above, one might expect penetratin to be a pore-forming peptide. It comes as a surprise, then, that penetratin behaves quite differently than the representative AMPs surveyed thus far.

Figure 8 shows a summary of X-ray diffraction and CD studies on penetratin mixed in four different lipid compositions (Lee *et al.* 2010). Like all AMPs we have studied, the penetratin binding causes membrane thinning in proportional to P/L, and there is also a critical P/L^* for the limit of linear thinning. But as P/L exceeds P/L^*, we observed behavior strikingly different from AMPs. Normally one expects pores appear in the membrane at $P/L > P/L^*$, but penetratin did not cause pore formation and no molecular leakage was detected from GUVs (Sun *et al.* 2010). Instead, penetratin transformed into a β-sheet structure at concentrations higher than P/L^* as shown by CD. Furthermore, the β-sheet penetratin aggregated and exited from the lipid

https://doi.org/10.1017/S0033583517000087

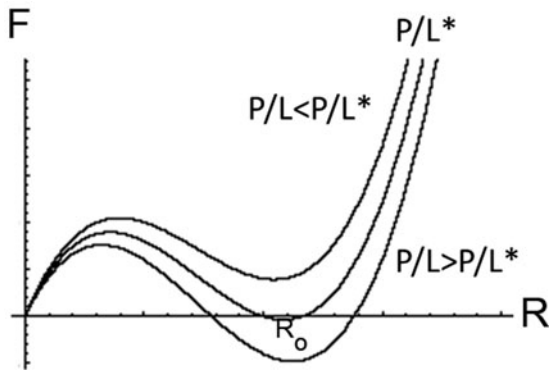

Fig. 7. The schematic drawing of the free energy of pore formation induced by AMP (Eq. 2). The minimum of the free energy is at radius $R = 0$ for $P/L < P/L^*$. But for $P/L > P/L^*$, the minimum of the free energy is at a finite R, indicating a stable pore formation. The transition for the pore formation occurs at $P/L = P/L^*$ (Huang *et al.* 2004).

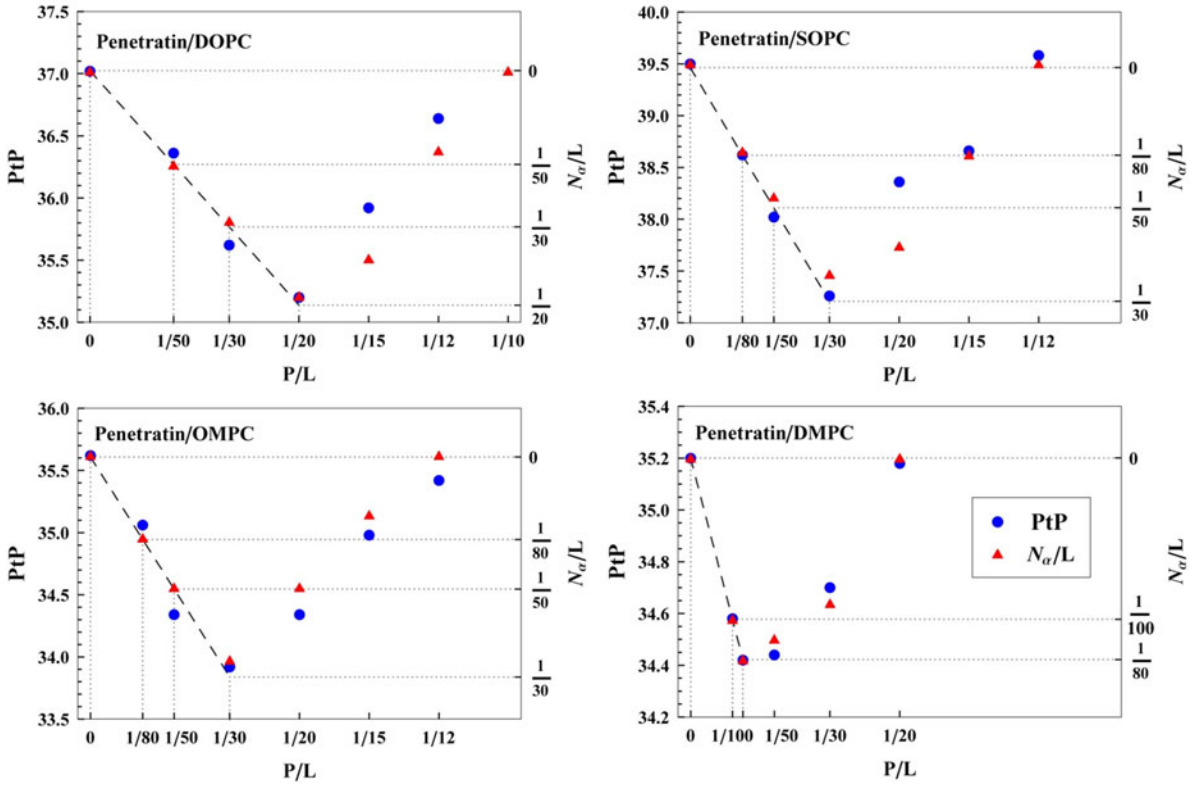

Fig. 8. Penetrain was studied in bilayers of four different lipid compositions as a function of the peptide to lipid ratio P/L. The bilayer thickness PtP and the fraction of penetratin in the α-helical form N_α/L (the remaining in the β-sheet form) were measured. The lowest PtP point defines P/L^*. For $P/L<P/L^*$, there is a linear relation between PtP and P/L as shown by the dash line (a linear fit) and the peptide is 100% α-helical. The coordinate of N_α/L (shown on the right-hand ordinate) was chosen to coincide with the P/L value on the dash line so that there is a one-to-one correspondence between the PtP value and the N_α/L value. The agreement between PtP and N_α/L for $P/L > P/L^*$ supports the assumption that membrane thinning was due to the α-helical bound peptides and that the peptides in the β conformation did not affect the membrane thickness. The peptide in β conformation exited from the lipid bilayer (Lee *et al.* 2010).

bilayer, such that the bilayer eventually recovered its free-bilayer thickness when all of penetratin transformed into β-sheet aggregates.

Corresponding GUV experiments showed that when the GUV membrane area expansion reached $\Delta A/A = 1.6 \pm 0.5\%$., penetratin helices transformed into visible aggregates that exited from the outer leaflet of the GUV (Sun *et al.* 2010). In multilayer samples penetratin was mixed in both sides of bilayers, membrane thinning reached $-\Delta h/h = 4.7 \pm 0.5\%$, before penetratin

https://doi.org/10.1017/S0033583517000087

helices transformed to β-sheet aggregates and exited from both sides of the lipid bilayers. Unlike melittin and the other AMPs we have studied, penetratin experiments showed no correlations between the membrane thinning in multilayers and the GUV membrane area expansion. This suggests that penetratin does not translocate across the bilayer like AMPs. This observation corroborates the idea that AMPs' propensity for pore formation enables their translocation across a bilayer by transient pores even at very low AMP concentration; whereas penetration does not.

Thus, penetratin is a proof that there is a criterion for a cationic, amphipathic peptide to be a pore-forming peptide that is yet to be determined (Boman *et al.* 1994). We have found that all amphipathic peptides initially bind to the interface of membranes as monomers and cause membrane thinning. As we argued above, the membrane thinning effect causes the chemical potential of the peptide to increase with P/L, equivalently the free energy of the peptide-lipid system increases with $(P/L)^2$ (relative to the initial state of no binding). At a certain value of P/L, some other configuration of the peptide-lipid system may have a lower free energy than the state of membrane with monomeric peptides bound on its planar interface. For AMPs, this lower free energy state is for the peptides remaining α-helical but the membrane transforms to a state with pores where multiple peptides bound on the inner surface of the pores. For penetratin, however, the lower free energy state is one in which initially α-helical peptides transform into β-sheet aggregates and exit from the membrane.

Ultimately, the experimental and theoretical investigations outlined in this paper are all based on the belief that interactions of AMPs with membranes are best described by considering the evolution of a peptide-membrane system. The soft matter properties of this system may be investigated using microscopy and optical experiments as well as the traditional methods of solid state physics such as neutron and X-ray scattering/diffraction. We believe that we have demonstrated the basic principles for understanding the mechanism of common AMPs, often taking melittin as a representative example. Yet, there are other membrane-active peptides and agents, which are not describable using this seemingly general pore-forming model. The case of penetratin shows that remarkably similar peptides can display very different behavior in the membrane. Just as well, the cyclic lipopeptide daptomycin and the antifungal macrolide amphotericin B are not described by the AMP model.

Still, it is evident that experiments on these molecules that are guided by such a conceptual and experimental framework for studying pore-forming AMPs may reveal many unique properties and phenomena. We believe it is of interest to pursue novel research with both familiar and mysterious membrane-active peptides guided by the results obtained from pore-forming AMP studies.

Supplementary material

The supplementary material for this article can be found at https://doi.org/10.1017/S0033583517000087.

Acknowledgements

This work was supported by the NIH (US) Grant GM55203 and the Robert A. Welch Foundation Grant C-0991.

References

Barns, K. J. & Weisshaar, J. C. (2013). Real-time attack of LL-37 on single Bacillus subtilis cells. *Biochimica et Biophysica Acta* **1828**(6), 1511–1520.

Baumann, G. & Mueller, P. (1974). A molecular model of membrane excitability. *Journal of Supramolecular Structure* **2**(5–6), 538–557.

Bierbaum, G. & Sahl, H. G. (1987). Autolytic system of Staphylococcus simulans 22: influence of cationic peptides on activity of N-acetylmuramoyl-L-alanine amidase. *Journal of Bacteriology* **169**(12), 5452–5458.

Boman, H. G. & Hultmark, D. (1987). Cell-free immunity in insects. *Annual Review of Microbiology* **41**, 103–126.

Boman, H. G., Marsh, J. & Goode, J. A. (eds) (1994). *Antimicrobial Peptides*. Chichester: John Wiley and Sons.

Brochard-Wyart, F., De Gennes, P. G. & Sander, O. (2000). Transient pores in stretched vesicles: role of leak-0ut. *Physica A* **278**, 32–51.

Christensen, B., Fink, J., Merrifield, R. B. & mauzerall, D. (1988). Channel-forming properties of cecropins and related model compounds incorporated into planar lipid membranes. *Proceedings of the National Academy of Sciences USA* **85**(14), 5072–5076.

Debye, P. (1949). Light scattering in soap solutions. *Annals of the New York Academy of Sciences*. **51**, 575–592.

Degrado, W. F., Kezdy, F. J. & Kaiser, E. T. (1981). Design, synthesis and characterization of a cytotoxic peptide with melittin-like activity. *Journal of the American Chemical Society* **103**, 679–681.

Duchardt, F., Fotin-Mleczek, M., Schwarz, H., Fischer, R. & Brock, R. (2007). A comprehensive model for the cellular uptake of cationic cell-penetrating peptides. *Traffic* **8**(7), 848–866.

Duclohier, H., Molle, G. & Spach, G. (1989). Antimicrobial peptide magainin I from Xenopus skin forms anion-permeable channels in planar lipid bilayers. *Biophysical Journal* **56**(5), 1017–1021.

Elsbach, P. & Weiss, J. (1993). Bactericidal/permeability increasing protein and host defense against gram-negative bacteria and endotoxin. *Current Opinion in Immunology* **5**(1), 103–107.

Fantner, G. E., Barbero, R. J., Gray, D. S. & Belcher, A. M. (2010). Kinetics of antimicrobial peptide activity measured on individual bacterial cells using high-speed atomic force microscopy. *Nature Nanotechnology* **5**(4), 280–285.

Faust, J. E., Yang, P. Y. & Huang, H. W. (2017). Action of antimicrobial peptides on bacterial and lipid membranes: a direct comparison. *Biophysical Journal* **112**, 1–10.

Fischer, R., Fotin-Mleczek, M., Hufnagel, H. & Brock, R. (2006). Break on through to the other side-biophyiscs and cell biology shet light on cell-penetrating peptides. *Chembiochem* **6**, 2126–2142.

Fox, Jr., R. O., & Richards, F. M. (1982). A voltage-gated ion channel model inferred from the crystal structure of alamethicin at 1·5-A resolution. *Nature* **300**(5890), 325–330.

Fuertes, G., Garcia-Saez, A. J., Esteban-Martin, S., Gimenez, D., Sanchez-Munoz, O. L., Schwille, P. & Salgado, J. (2010). Pores formed by baxalpha5 relax to a smaller size and keep at equilibrium. *Biophysical Journal* **99**(9), 2917–2925.

Gazit, E., Boman, A., Boman, H. G. & Shai, Y. (1995). Interaction of the mammalian antibacterial peptide cecropin P1 with phospholipid vesicles. *Biochemistry* **34**(36), 11479–11488.

Gazit, E., Lee, W. J., Brey, P. T. & Shai, Y. (1994). Mode of action of the antibacterial cecropin B2: a spectrofluorometric study. *Biochemistry* **33**(35), 10681–10692.

Gordon, L. G. & Haydon, D. A. (1972). The unit conductance channel of alamethicin. *Biochimica et Biophysica Acta* **255**(3), 1014–1018.

Hanke, W., Methfessel, C., Wilmsen, H. U., Katz, E., Jung, G. & Boheim, G. (1983). Melittin and a chemically modified trichotoxin form alamethicin-type multi-state pores. *Biochimica et Biophysica Acta* **727**(1), 108–114.

He, K., Ludtke, S. J., Huang, H. W. & Worcester, D. L. (1995). Antimicrobial peptide pores in membranes detected by neutron in-plane scattering. *Biochemistry* **34**(48), 15614–15618.

He, K., Ludtke, S. J., Worcester, D. L. & Huang, H. W. (1996). Neutron scattering in the plane of membranes: structure of alamethicin pores. *Biophysical Journal* **70**(6), 2659–2666.

Helfrich, W. (1973). Elastic properties of lipid bilayers: theory and possible experiments. *Zeitschrift fur Naturforschung* **28c**, 693–703.

Heller, W. T., Waring, A. J., Lehrer, R. I., Harroun, T. A., Weiss, T. M., Yang, L. & Huang, H. W. (2000). Membrane thinning effect of the beta-sheet antimicrobial protegrin. *Biochemistry* **39**(1), 139–145.

Heller, W. T., Waring, A. J., Lehrer, R. I. & Huang, H. W. (1998). Multiple states of beta-sheet peptide protegrin in lipid bilayers. *Biochemistry* **37**(49), 17331–17338.

Hirsh, D. J., Hammer, J., Maloy, W. L., Blazyk, J. & Schaefer, J. (1996). Secondary structure and location of a magainin analogue in synthetic phospholipid bilayers. *Biochemistry* **35**(39), 12733–12741.

Huang, H. W. (1986). Deformation free energy of bilayer membrane and its effect on gramicidin channel lifetime. *Biophysical Journal* **50**, 1061–1071.

Huang, H. W. (1995). Elasticity of lipid bilayer interaction with amphiphilic helical peptides. *Journal de Physique II France* **5**, 1427–1431.

Huang, H. W. (2000). Action of antimicrobial peptides: two-state model. *Biochemistry* **39**(29), 8347–8352.

Huang, H. W. (2009). Free energies of molecular bound states in lipid bilayers: lethal concentrations of antimicrobial peptides. *Biophysical Journal* **96**(8), 3263–3272.

Huang, H. W., Chen, F. Y. & Lee, M. T. (2004). Molecular mechanism of peptide induced pores in membranes. *Physical Review Letters* **92**, 198301–198304.

Huang, H. W. & Wu, Y. (1991). Lipid-alamethicin interactions influence alamethicin orientation. *Biophysical Journal* **60**, 1079–1087.

Karatekin, E., Sandre, O., Guitouni, H., Borghi, N., Puech, P. H. & Brochard-Wyart, F. (2003). Cascades of transient pores in giant vesicles: line tension and transport. *Biophysical Journal* **84**(3), 1734–1749.

Landau, L. D. A. L. & Lifshitz, E. M. (1965). *Statistical Physics*. New York: Pergamon Press.

Last, N. B. & Miranker, A. D. (2013). Common mechanism unites membrane poration by amyloid and antimicrobial peptides. *Proceedings of the National Academy of Sciences USA* **110**(16), 6382–6387.

Latorre, R. & Alvarez, O. (1981). Voltage-dependent channels in planar lipid bilayer membranes. *Physiological Reviews* **61**(1), 77–150.

Lee, C. C., Sun, Y. & Huang, H. W. (2010). Membrane-mediated peptide conformation change from alpha-monomers to beta-aggregates. *Biophysical Journal* **98**(10), 2236–2245.

Lee, C. C., Sun, Y., Qian, S. & Huang, H. W. (2011). Transmembrane pores formed by human antimicrobial peptide LL-37. *Biophysical Journal* **100**(7), 1688–1696.

Lee, M. T., Chen, F. Y. & Huang, H. W. (2004). Energetics of pore formation induced by membrane active peptides. *Biochemistry* **43**(12), 3590–3599.

Lee, M. T., Hung, W. C., Chen, F. Y. & Huang, H. W. (2005). Many-body effect of antimicrobial peptides: on the correlation between lipid's spontaneous curvature and pore formation. *Biophysical Journal* **89**(6), 4006–4016.

Lee, M. T., Hung, W. C., Chen, F. Y. & Huang, H. W. (2008). Mechanism and kinetics of pore formation in membranes by water-soluble amphipathic peptides. *Proceedings of the National Academy of Sciences USA* **105**(13), 5087–5092.

Lee, M. T., Sun, T. L., Hung, W. C. & Huang, H. W. (2013). Process of inducing pores in membranes by melittin. *Proceedings of the National Academy of Sciences USA* **110**(35), 14243–14248.

Litster, J. D. (1975). Stability of lipid bilayers and red blood cell membranes. *Physics Letters A* **53**, 193–194.
Ludtke, S., He, K. & Huang, H. (1995). Membrane thinning caused by magainin 2. *Biochemistry* **34**(51), 16764–16769.
Ludtke, S. J., He, K., Heller, W. T., Harroun, T. A., Yang, L. & Huang, H. W. (1996). Membrane pores induced by magainin. *Biochemistry* **35**(43), 13723–13728.
Ludtke, S. J., He, K., Wu, Y. & Huang, H. W. (1994). Cooperative membrane insertion of magainin correlated with its cytolytic activity. *Biochimica et Biophysica Acta* **1190**(1), 181–184.
Mak, D. O. & Webb, W. W. (1995). Two classes of alamethicin transmembrane channels: molecular models from single-channel properties. *Biophysical Journal* **69**(6), 2323–2336.
Matsuzaki, K., Murase, O., Fujii, N. & Miyajima, K. (1995). Translocation of a channel-forming antimicrobial peptide, magainin 2, across lipid bilayers by forming a pore. *Biochemistry* **34**(19), 6521–6526.
Matsuzaki, K., Murase, O., Fujii, N. & Miyajima, K. (1996). An antimicrobial peptide, magainin 2, induced rapid flip-flop of phospholipids coupled with pore formation and peptide translocation. *Biochemistry* **35**(35), 11361–11368.
Matsuzaki, K., Yoneyama, S. & Miyajima, K. (1997). Pore formation and translocation of melittin. *Biophysical Journal* **73**(2), 831–838.
Melikov, K. & Chernomordik, L. V. (2005). Arginine-rich cell penetrating peptides: from endosomal uptake to nuclear delivery. *Cellular and Molecular Life Sciences* **62**(23), 2739–2749.
Merrifield, R. B., Merrifield, E. L., Juvvadi, P., Andreu, D. & Boman, H. G. (1994a). Design and synthesis of antimicrobial peptides. In *Antimicrobial Peptides* (eds. H. G. Boman, J. Marsh & J. A. Goode), pp. 5–26. Chichester: John Wiley & Sons.
Merrifield, R. B., Merrifield, E. L., Juvvadi, P., Andreu, D. & Boman, H. G. (1994b). Design and synthesis of antimicrobial peptides. In *Ciba Foundation Symposium 186* (eds. H. G. Boman, J. Marsh & J. A. Goodel), pp. 5–26. John Wiley.
Moon, C. P. & Fleming, K. G. (2011). Side-chain hydrophobicity scale derived from transmembrane protein folding into lipid bilayers. *Proceedings of the National Academy of Sciences USA* **108**(25), 10174–10177.
Mueller, P. & Rudin, D. O. (1968). Action potentials induced in biomolecular lipid membranes. *Nature* **217**(5130), 713–719.
Nomura, F., Nagata, M., Inaba, T., Hiramatsu, H., Hotani, H. & Takiguchi, K. (2001). Capabilities of liposomes for topological transformation. *Proceedings of the National Academy of Sciences USA* **98**(5), 2340–2345.
Olah, G. A., Huang, H. W., Liu, W. H. & Wu, Y. L. (1991). Location of ion-binding sites in the gramicidin channel by X-ray diffraction. *Journal of Molecular Biology* **218**(4), 847–858.
Pogliano, J., Pogliano, N. & Silverman, J. A. (2012). Daptomycin-mediated reorganization of membrane architecture causes mislocalization of essential cell division proteins. *Journal of Bacteriology* **194**(17), 4494–4504.
Puech, P. H., Borghi, N., Karatekin, E. & Brochard-Wyart, F. (2003). Line thermodynamics: adsorption at a membrane edge. *Physical Review Letters* **90**, 128301–128304.
Qian, S., Wang, W., Yang, L. & Huang, H. W. (2008a). Structure of the alamethicin pore reconstructed by X-ray diffraction analysis. *Biophysical Journal* **94**, 3512–3522.
Qian, S., Wang, W., Yang, L. & Huang, H. W. (2008b). Structure of transmembrane pore induced by Bax-derived peptide: evidence for lipidic pores. *Proceedings of the National Academy of Sciences USA* **105**(45), 17379–17383.
Qian, Y. Q., Billeter, M., Otting, G., Muller, M., Gehring, W. J. & Wuthrich, K. (1989). The structure of the Antennapedia homeodomain determined by NMR spectroscopy in solution: comparison with prokaryotic repressors. *Cell* **59**(3), 573–580.
Rangarajan, N., Bakshi, S. & Weisshaar, J. C. (2013). Localized, persistent permeabilization of *E. coli* membranes by the antimicrobial peptide cecropin A. *Biochemistry* **52**, 6584–6594.
Ruthe, H. J. & Adler, J. (1985). Fusion of bacterial spheroplasts by electric fields. *Biochimica et Biophysica Acta* **819**(1), 105–113.
Safinya, C. R., Sirota, E. B., Roux, D. & Smith, G. S. (1989). Universality in interacting membranes – the effect of cosurfactants on the interfacial rigidity. *Physical Review Letters* **62**(10), 1134–1137.
Schümann, M., Dathe, M., Wieprecht, T., Beyermann, M. & Bienert, M. (1997). The tendency of magainin to associate upon binding to phospholipid bilayers. *Biochemistry* **36**, 4345–4351.
Sochacki, K. A., Barns, K. J., Bucki, R. & Weisshaar, J. C. (2011). Real-time attack on single *Escherichia coli* cells by the human antimicrobial peptide LL-37. *Proceedings of the National Academy of Sciences USA* **108**(16), E77–E81.
Steiner, H., Andreu, D. & Merrifield, R. B. (1988). Binding and action of cecropin and cecropin analogues: antibacterial peptides from insects. *Biochimica et Biophysica Acta* **939**(2), 260–266.
Sun, Y., Lee, C. C., Chen, T. H. & Huang, H. W. (2010). Kinetic process of beta-amyloid formation via membrane binding. *Biophysical Journal* **99**(2), 544–552.
Sun, Y., Sun, T. L. & Huang, H. W. (2014). Physical properties of *Escherichia coli* spheroplast membranes. *Biophysical Journal* **107**(9), 2082–2090.
Sun, Y., Sun, T. L. & Huang, H. W. (2016). Mode of action of antimicrobial peptides on *E. coli* spheroplasts. *Biophysical Journal* **111**(1), 132–139.
Tamba, Y. & Yamazaki, M. (2005). Single giant unilamellar vesicle method reveals effect of antimicrobial peptide magainin 2 on membrane permeability. *Biochemistry* **44**(48), 15823–15833.
Taupin, C., Dvolaitzky, M. & Sauterey, C. (1975). Osmotic pressure induced pores in phospholipid vesicles. *Biochemistry* **14**(21), 4771–4775.
Terwilliger, T. C., Weissman, L. & Eisenberg, D. (1982). The structure of melittin in the form I crystals and its implication for melittin's lytic and surface activities. *Biophysical Journal* **37**(1), 353–361.
Tosteson, M. T. & Tosteson, D. C. (1981). The sting. Melittin forms channels in lipid bilayers. *Biophysics Journal* **36**(1), 109–116.

https://doi.org/10.1017/S0033583517000087

Urbaneja, M. A., Goni, F. M. & Alonso, A. (1988). Structural changes induced by Triton X-100 on sonicated phosphatidylcholine liposomes. *European Journal of Biochemistry* **173**(3), 585–588.

Urrutia, R., Cruciani, R. A., Barker, J. L. & Kachar, B. (1989). Spontaneous polymerization of the antibiotic peptide magainin 2. *FEBS Letters* **247**(1), 17–21.

Wack, D. C. & Webb, W. W. (1989). Measurement by X-ray diffraction methods of the layer compressional elastic constant B in the lyotropic smectic-A (L-alpha) phase of the lecithin-water system. *Physics Review A* **40**, 1627–1636.

Wade, D., Boman, A., Wahlin, B., Drain, C. M., Andreu, D., Boman, H. G. & Merrifield, R. B. (1990). All-D amino acid-containing channel-forming antibiotic peptides. *Proceedings of the National Academy of Sciences USA* **87**(12), 4761–4765.

Weiss, T. M., Van Der Wel, P. C., Killian, J. A., Koeppe, II, R. E., & Huang, H. W. (2003). Hydrophobic mismatch between helices and lipid bilayers. *Biophysical Journal* **84**(1), 379–385.

Wu, Y., Huang, H. W. & Olah, G. A. (1990). Method of oriented circular dichroism. *Biophysical Journal* **57**, 797–806.

Yang, L., Harroun, T. A., Heller, W. T., Weiss, T. M. & Huang, H. W. (1998). Neutron off-plane scattering of aligned membranes. I. Method of measurement. *Biophysical Journal* **75**(2), 641–645.

Yang, L., Harroun, T. A., Weiss, T. M., Ding, L. & Huang, H. W. (2001). Barrel-stave model or toroidal model? a case study on melittin pores. *Biophysical Journal* **81**, 1475–1485.

Yang, L., Weiss, T. M., Harroun, T. A., Heller, W. T. & Huang, H. W. (1999). Supramolecular structures of peptide assemblies in membranes by neutron off-plane scattering: method of analysis. *Biophysical Journal* **77**(5), 2648–2656.

Yang, L., Weiss, T. M. & Huang, H. W. (2000). Crystallization of antimicrobial pores in membranes: magainin and protegrin. *Biophysical Journal* **79**, 2002–2009.

Zasloff, M. (1987). Magainins, a class of antimicrobial peptides from Xenopus skin: isolation, characterization of two active forms, and partial cDNA sequence of a precursor. *Proceedings of the National Academy of Sciences USA* **84**(15), 5449–5453.

Zasloff, M. (2002). Antimicrobial peptides of multicellular organisms. *Nature* **415**(6870), 389–395.

https://doi.org/10.1017/S0033583517000087

Supplemental Information

Understanding Membrane-active Antimicrobial Peptides

Huey W. Huang and Nicholas E. Charron
Department of Physics and Astronomy, Rice University, Houston, Texas 77005

This supplemental information provides comments on sample preparation and experimental procedures for the studies that have been done in support of this review. We feel that it is important to reiterate and demonstrate the importance of sample preparation and quality, as well as some not commonly discussed aspects of the associated methods. We focus primarily on the techniques related to multilayer samples, as structure/state determination of a soft matter peptide-membrane system is susceptible to several subtle but important pitfalls.

S1. Comments on sample preparation

Good sample quality is crucial for the success of experiments that investigate membrane active agents. This is in part due to the inherent difficulty of studying single membranes with traditional physical techniques. In particular, a single bilayer supported on a solid substrate is known to have its properties altered from that of a free bilayer in solution (Hemmerle et al., 2012). An ideal alternative is a stack of parallel bilayers of lipid-peptide mixtures separated by water layers, equivalent to a smectic liquid crystal. However, lipids have a molecular basis for a very rich lyotropic liquid crystal phase diagram that depends heavily on both temperature and hydration. There are many types of defects that can span over a variety of length scales. Due to the birefringence of optical artifacts, polarizing microscopy can be used to qualitatively identify and characterize defects in multilayer samples (Powers & Pershan, 1977). X-ray can also be used to measure sample alignment and homogeneity, as well as detecting the formation of phase domains. Thus rejection of poor samples should be a routine and well-defined process in X-ray, neutron, and OCD experiments.

The quality of GUVs is a little less straightforward to ascertain. GUVs seem to be considerably more fragile than biological membranes (the reason for which is still not entirely certain) (Faust et al., 2017). GUVs with diameters on the order of one to tens of microns should be able to withstand reversible membrane tensions on the order of mN/m (Lee et al, 2013). GUVs are typically produced in ~ 200 mM sucrose (or glucose) and immersed in ~200 mM glucose (or sucrose) solution. The high concentrations of sugar control the osmolalities so as to withstand modest osmotic downshifts and upshifts. The choice of sucrose and glucose provides phase contrast for microscopic observation and also provide a density differential to control the vertical position of GUVs in the observation chamber.

Multilayer Sample Preparation

As stated earlier, well defined sample preparation is key to studying AMPs with precision. Methods such as X-ray diffraction and OCD require uniform and well-aligned samples to provide good signal to noise ratios, and the accurate extraction of peptide behaviors from these techniques

require good sample alignment. X-ray diffraction is especially sensitive to sample quality, and direct measurements can unambiguously detect samples with poor alignment, non-uniformity or phase separations.

Generally, there are two methods for diffraction/OCD multilayer sample preparation. The first involves the use of organic solvents to mix and spread compounds on substrates (silicon wafer, glass, or quartz). Lipids and additional components are first co-dissolved in a mixture of organic solvents and pipetted onto cleaned substrate. Either by hand or by some form of auto-nutation/rotation, the substrates carrying the deposited solution can be gently rocked or gyrated to spread the sample evenly while the solvents evaporate. Liquid surface tension and contact angle play a critical role in this process; the ideal solution is tensionless to allow for natural spreading across the substrate, so solvents may be chosen at ratios that produce this characteristic behavior (Ludtke et al., 1995). Generally, a hydrophobic solvent can be used to dissolve the lipid-peptide mixture, while an amphipathic solvent promotes sufficient spreading over the substrate surface. Common solvent choices are chloroform, trifluoroethanol, and/or methanol.

After most of the solvent has evaporated and the sample is uniformly distributed on the substrate, the substrate may be set aside to allow the remainder of the solvent to evaporate. It is usually necessary to remove all traces of the solvent after spreading, so samples are placed under vacuum for at least an hour after the mixing. Once all of the solvent has been removed, the substrates with dried sample are incubated and slowly rehydrated in the presence of purified water vapor (preferably over night), after which they may be mounted for diffraction or OCD experiments.

A major caveat for preparing multilayer samples with organic solvents is solubility. In order to produce well-mixed samples, all components must be soluble in the final solvent mixture. For simple mixtures and samples of pure lipid this is hardly an issue. However, more complicated lipid-peptide-sterol systems can often present the experimenter with a difficult problem in miscibility. Just as well, additional components, such as ions, may not be well incorporated using organic solvent methods and the uniformity of their distributions throughout the sample is not guaranteed. Additionally, mixed solvents with different evaporation rates may leave an experimenter with an initially well mixed sample that evolves to a poorly mixed one. Often the solution to this problem involves substantial trial and error concerning solvent types and mixing ratios.

The second method of multilayer preparation addresses some of these issues. This method involves the lyophilization of the sample into a powder form that may subsequently be rehydrated (Huang & Olah, 1987; Olah et al., 1991). First, dissolved lipids are dried down to a film and placed under vacuum. Next, the lipid film is mixed with some volume of pure water and is vortexed and sonicated to produce vesicles. Additional components, such as peptides, ions, or sterols, may be spiked in the resulting solution. This solution is vortexed and sonicated yet again to produce a uniform distribution. The solution is then frozen in preparation for lyophilization. Once frozen, the solution is placed under a cold vacuum until all water content is removed via sublimation and an anhydrous powder is produced. Typically, this process may be done

overnight. The resulting dried samples may be incubated and rehydrated with pure water to form a translucent gel-like substance. It is important to note that this hydration must be sufficiently quasi-static; if the hydration is too sudden (as a result from, for example, water droplets landing directly on the anhydrous powder), then a colloidal suspension of vesicles will be produced, instead of a well-aligned sample. This is often evidenced by a sticky and viscous solution that is opaque, off-white in color, rather than a translucent and easily partitionable gel.

The rehydrated lyophilized samples may be spread onto substrate using a small spatula. Gentle spreading will result in a visibly uniform conic-fan texture that is characteristic of the lipids' smectic liquid crystalline behavior (Kumar, 2001). Depending on the lipid mixture, the spreading process may be augmented by use of a glovebox with ambient humidity control and a controllable heater that makes thermal contact with the substrate. Alternatively, rehydrated samples may be sandwiched between two clear substrates (for OCD or neutron) or polished beryllium plates (X-ray) that are gently rubbed together with slight compression. This gentle pressure and rubbing can be used to localize multilayer defects to the edges of the substrate, and the presence of two bounding surfaces promotes the propagation of uniform lamellar order across the sample (Powers & Pershan, 1977). Samples that have been spread may be stored in incubation and further hydrated using pure water vapor in the same fashion as the samples prepared via organic solvents.

If the samples are prepared on glass, the alignment and domain quality may be investigated with the use of a polarizing microscope (Huang & Olah, 1987; Powers & Pershan, 1977). Lamellar lyotropics show clear birefringence associated with axes parallel and perpendicular to the layer normal. Lamellar X-ray diffraction can also measure sample quality, as a well-aligned sample will have a good signal to noise ratio, and, at less than full hydration, typically more than four Bragg orders with sharp diffraction peaks. A θ–2θ scan can reveal any phase separation--a phenomenon marked by the appearance of more than one series of peaks with different repeat distances. The mosaic quality may be more carefully inspected with a two-dimensional rocking (ω, θ) scan centered about a chosen Bragg peak. A sample that has poor layer alignment shows no omega dependence in the intensity of the scan, a feature characteristic of powder samples, and is marked by the appearance of an extremely wide Gaussian peak along the omega axis. By contrast, a well aligned sample has a sharp omega dependence in the intensity that is focused in a narrow Gaussian peak about the center of the Bragg peak under inspection (Weiss et al., 2003).

S2. Comments on methods

S2.1 GUV in peptide solution—aspiration method

The aspiration method (Kwok & Evans, 1981) measures the membrane area change by peptide binding, from which one can find, by its correlation with the membrane thinning effect measured with X-ray diffraction, the number of peptides bound to the GUV membrane (the bound peptide to lipid ratio) during the experiment (Sun et al., 2009)).

When a GUV is exposed to pore-forming peptides, the initial binding of peptides always expands the membrane area of the GUV, resulting in an increased protrusion length in the

aspiration micropipette (Lee et al., 2008; Longo et al., 1998; Longo et al., 1997; Sun et al., 2009). The simplest explanation for this is that additional molecules have been incorporated into the lipid bilayer. The subsequent pore formation causes a net water influx if, for example, sucrose and glucose are used as the solutes inside and outside the GUV, respectively. This would cause a decreased protrusion length (Lee et al., 2011; Lee et al., 2013; Longo et al., 1998; Longo et al., 1997; Sun et al., 2009), because glucose is smaller than sucrose, leading to a slightly larger glucose influx than a sucrose eflux which in turn produces a net water influx due to osmolality imbalance (Longo et al., 1998). If the sucrose and glucose were exchanged, the pore formation would cause a net water efflux, resulting in an increased protrusion length (Sun et al., 2009).

S2.2 Measurement of instantaneous membrane permeability

Membrane permeability induced by AMPs is most commonly measured by molecular leak-in or leak-out methods (Fuertes et al., 2010; Tamba et al., 2010; Tamba & Yamazaki, 2005). For instance, the time curve for the dye release can be measured from a GUV or from a population of small vesicles. However, the membrane permeability induced by AMPs in solution changes with time, as the peptides gradually bind to the membrane. A single time curve of efflux or influx does not reveal such time dependent changes. If it is the collective efflux from a population of small vesicles, the kinetics can be complicated by the ensemble average and by the molecular exchange between vesicles by collision (Martin & Pagano, 1987; Rodriguez et al., 2005; Seigneuret & Devaux, 1984). In (Faust et al., 2017; Sun et al., 2016), we have shown that, by photobleaching and fluorescence recovery in a leak-in experiment, we can measure the instantaneous permeability in a bacterial membrane by using spheroplasts or in a lipid bilayer by using GUVs.

S2.3 Oriented circular dischroism (OCD)

The method of OCD is perhaps the simplest way of measuring the configuration and orientation of peptides in membranes (Wu et al., 1990). Other methods that have been used for the same purpose include solid-state NMR (Bechinger et al., 1991; Glaser et al., 2004) and polarized infrared spectroscopy (Rothschild et al., 1980; Tamm & Tatulian, 1997). For the comparison of the uses of OCD and ssNMR, see (Burck et al., 2008).

The UV CD spectra of polypeptides and proteins are dominated by the electronic transitions in the peptide backbone and are relatively independent of the side chains. The asymmetric and periodic arrangements of peptide units in secondary structures give rise to characteristic CD spectra. In particular, the α-helix conformation has a highly distinctive spectrum. Within the UV range of commercial CD spectrometers ($\sim 185 - 240\ nm$), the helical spectrum is dominated by the π-π^* and n- π^* transitions (Woody, 1985). According to the exciton theory of Moffitt (Moffitt, 1956), the π-π^* transition in an α-helix is split into components with polarization either perpendicular or parallel to the helical axis. This theory was difficult to prove experimentally due to the difficulty of aligning a sample of α-helices. The use of long polypeptides in an electric field led to conflicting results (Yamaoka et al., 1986), because the

bending of long polypeptides was not taken into account (Olah & Huang, 1988a). Moffitt's prediction on polarization was finally demonstrated experimentally by using membrane-spanning α-helices aligned in lipid multilayers (Olah & Huang, 1988a; Olah & Huang, 1988b). Indeed, stacked lipid bilayers provides an ideal scaffolding for aligning short peptides and membrane-spanning proteins. Clearly the method used to prove the Moffitt theory can be utilized to measure the orientation of the helical sections of membrane proteins. The theoretical basis for the OCD method is given in Wu et al. (Wu et al., 1990). Here we provide some practical information for the use of OCD.

OCD of α-helices

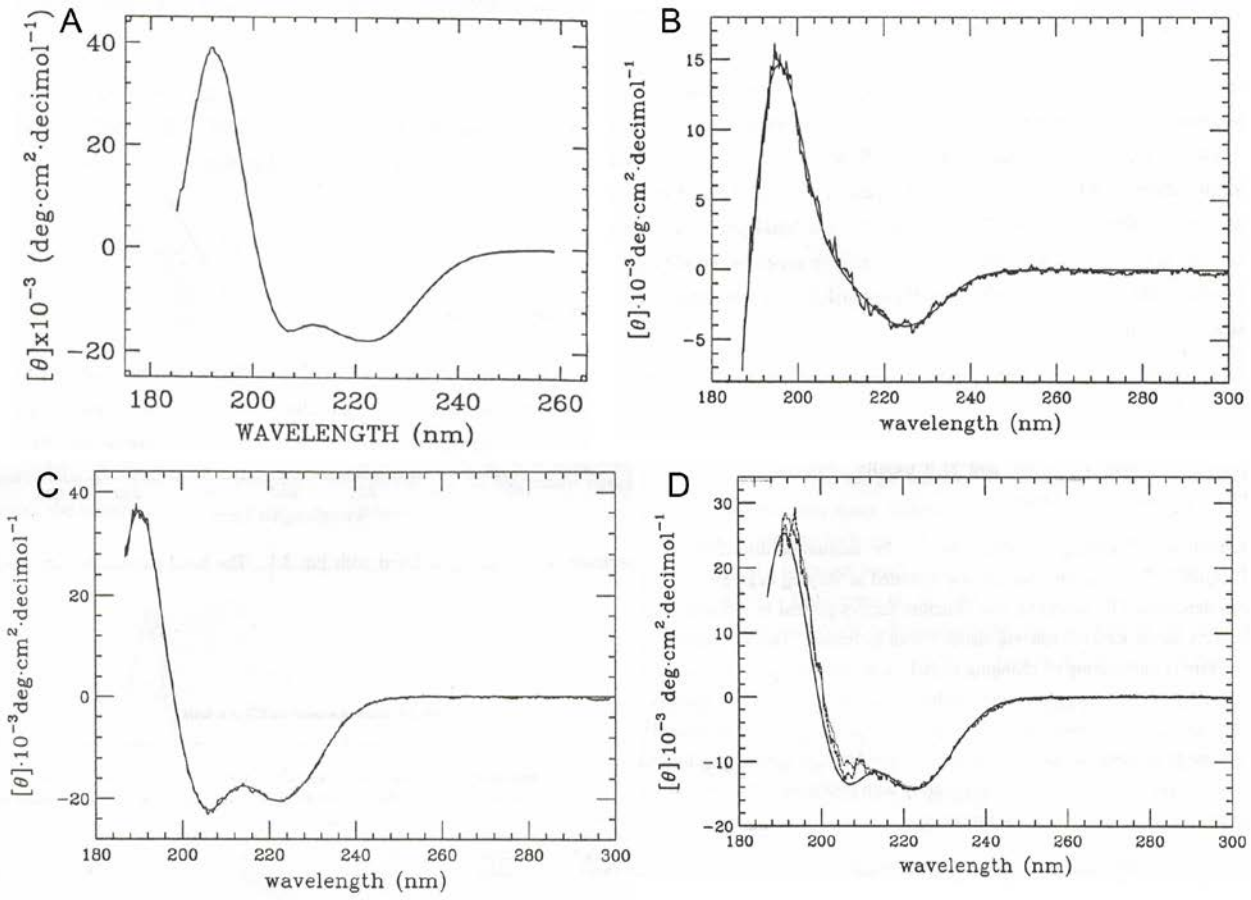

Figure S1 Solution CD and OCD of alamethicin. (A) The solution CD of alamethicin embedded in DPhPC vesicles. (B) OCD of alamethicin in DPhPC multilayers in full hydration. Alamethicin helix is oriented perpendicular to the plane of bilayers—this is called the I state. (C) OCD of alamethicin in DPhPC multilayers in low hydration (~ 50% RH). Alamethicin helix is oriented parallel to the plane of membrane—this is called the S state. (D) The solution CD is the rotational average of the S and I state: $(\frac{1}{3}I + \frac{2}{3}S)$ constructed from (B) and (C) shown in dotted line, compared with the directly measured solution CD in solid line (same as A).

Fig. S1 (Wu et al., 1990) shows the solution CD of alamethicin embedded in lipid vesicles. The negative CD band near 224 nm is due to the n-π^* transition of a magnetic dipole transition moment directed along the carbonyl bond in the helix; the band is approximately a Gaussian. The π-π^* transition in a helix, however, splits into three: one has its electric transition dipole polarized parallel to the helical axis and gives rise to the negative Gaussian band near 205 nm; the other two have their electric transition dipoles polarized perpendicular to the helical axis, giving rise to a positive Gaussian band near 190 nm when the incident light is perpendicular to the helical axis, but, when the incident light is parallel to the helical axis, the two transitions combine to produce the shape of the derivative of a Gaussian centered near 190 nm with the positive amplitude on the long wavelength side called the helical band (Tinoco, 1964). (Note that the CD spectra of short helical peptides are similar but vary somewhat in the relative amplitudes of different bands—this variation does not affect the determination of orientation.)

In contrast to solution CD, OCD is measured with the incident light perpendicular to the oriented multilayers. An example of alamethicin in DPhPC is shown in Fig 9B and 9C (Wu et al., 1990). Alamethicin changes its orientation when the sample's hydration condition changes. At full hydration, the alamethicin helix is oriented perpendicular to the plane of bilayer; the incident light is parallel to the helical axis, the positive band near 190 nm is red shifted (the helical band has a negative band blue shifted to below 190 nm which is difficult to detect by commercial CD spectrometers), the 205 nm band diminishes and the 224 nm band becomes smaller compared with the solution CD—this is called the I state (Fig. 9B). At low hydration (~50% RH), alamethicin helix is oriented parallel to the plane of membrane, i.e., the incident light is perpendicular to the helical axis, there are one positive band at 190 nm, a negative band at 205 nm and a negative band at 224 nm (Fig. 9C). This is called the S state. In solution CD, the observed signal is the rotational average of the S and I state ($\frac{1}{3}I + \frac{2}{3}S$), which agrees with the directly measured solution CD (Fig. 9D). Because the amplitudes associated with S are larger than that of I, the S state is similar to the solution CD (the distinction is the more negative amplitude at 205 nm). If a peptide has only two stable orientations, then the OCD of any mixed state exists as a linear combination of the I and S states. (A mixed state can also be interpreted as a helix at a tilted angle (Wu et al., 1990), but we believe that a peptide having multiple stable tilt-angle states is unlikely.)

OCD of β-sheets.

The OCD theory for β-sheets is less well developed (Bazzi & Woody, 1987; Woody, 1993) compared with α-helices. Nevertheless OCD has been used to establish two distinct states of protegrin (Ding et al., 2003; Heller et al., 1998) and θ-defensins (Weiss et al., 2002) in membranes.

Practical OCD analysis.

Ideally one would like to obtain both the S and I spectra from one single sample, so that they are normalized relative to each other. In this case, the OCD of the peptide in any condition

can be decomposed into a linear combination of S and I states, from which the percent of the peptide in each orientation is determined. This is done by searching two extreme spectra in the sense that all other spectra fall in between and can be expressed as a linear combination of the two. The extreme spectra have been found by measuring the OCD of a peptide in different lipid bilayers, P/L ratios, degrees of hydration and temperatures (Heller et al., 1998; Huang & Wu, 1991; Ludtke et al., 1994; Weiss et al., 2002; Yang et al., 2001). One learns a great deal about the peptide of interest by these relatively simple measurements.

Even if one fails to obtain both S and I in one single sample, it is still possible to normalize S and I obtained from two different samples in different conditions by an isodichroic point. Suppose that there is a cross point between the mutually normalized S and I spectra, then this isodichroic point must be common to all spectra provided they are all normalized correctly. One can usually find such a point by varying the hydration or temperature of one sample. The relative normalization between different samples is then achieved by adjusting the ampltidues of all other spectra to cross this isodichroic point.

OCD distortion

The original paper on OCD discussed the possible artifacts of OCD measurement and the techniques for correction (Wu et al., 1990). In practice, the most common distortion of OCD spectra is due to sample defects. If the multiple bilayers in the sample are not well aligned (as determined by X-ray, for example), the OCD spectrum would appears normal, but the deduced peptide orientation would be erroneous. This is generally true for any method of peptide orientation measurement. Another commonly seen OCD distortion comes from a sample not spread uniformly over the substrate resulting in non-uniform thickness. In a severe case the amplitude would taper to zero as wavelength decreases. The following explanation makes this clear.

Modern CD spectroscopy is based on a polarization-modulation technique (Velluz et al., 1965). A linearly polarized light is modulated alternatively into the right and left circularly polarized light before passing through the sample. Thus the readout, i.e., the voltage output, consists of an AC component proportional to the AC component of the transmitted light I_{ac} and a DC component proportional to the average transmitted light I_{dc} ($I_{dc} >> I_{ac}$). The ellipticity is measured by the ratio of the AC component over the DC component I_{ac}/ I_{dc} (Velluz et al., 1965). This ingenious design makes the measured ellipticity (or CD) independent of the sample's optical absorption which increases drastically as the wavelength decreases below ~200 nm. Now, to illustrate the CD distortion by a non-uniform sample, imagine a sample does not cover the entire substrate, so the transmitted light consists of two parts, $(I_{ac} + I_{dc})_A$ and $(I_{dc})_B$; the B part has no AC component because it has no sample. The output of the CD measurement would then be $(I_{ac})_A/[(I_{dc})_A + (I_{dc})_B]$. As long as the sample absorption is relatively independent of wavelength this output would still produce a correct unnormalized CD spectrum (for example in the wavelength region above ~200 nm). However, below 200 nm the components $(I_{ac})_A$ and $(I_{dc})_A$ would exponentially decrease with the wavelength due to UV absorption by the sample, while the

component $(I_{dc})_B$ would remain as large as above 200 nm because there is no sample absorption. Thus, such a spectrum would be distorted.

S2.4 X-ray lamellar diffraction

There are two standard types of diffraction samples (Warren, 1990). One type is powder and another is crystalline. For lipid bilayers, a powder sample corresponds to collection of small multilayered vesicles. Diffraction peaks from such samples rarely show the full circles of diffraction patterns (as a perfect powder would), indicating a lack of isotropy, and are typically limited to 4 orders of Bragg peaks, which is insufficient for precise measurements. On the other hand, it is relatively easy to prepare the so-called "ideally imperfect" (Warren, 1990) smectic liquid crystalline samples as described in Section S1.

As mentioned previously, lamellar diffraction can be used to measure a peptide's effect on the thickness of the bilayer, its dependence on P/L, and the value of P/L*. Levine and Wilkins (Levine & Wilkins, 1971) carried out the first structural x-ray diffraction experiments on lipid bilayers, identifying distinct hydrocarbon chain and phosphate head group regions. The basic method exploits the one-dimensional periodicity of the multilamellar phase. In this liquid crystalline form, the unit cell is taken to be a bilayer and half of both sides of the surrounding water layers. These multilayer samples may be probed with simple θ–2θ scans.

The observed diffraction peaks must be adjusted with several physical and geometrical corrections. This first of these involves the removal of the background signal. The next correction applies to the absorption of the sample. This is perhaps one of the more difficult corrections to compute, as determining the exact number of parallel bilayers are present in the sample is nontrivial. However, if the thickness of the sample d is known, the absorption correction is simple (Warren, 1990): $C_{abs} = \left(\frac{sin\theta}{2\mu d}\left[1 - \exp\left(-\frac{2\mu d}{sin\theta}\right)\right]\right)$,

where μ, the sample absorption coefficient is simply the mass weighted sum of atomic coefficients based on the chemical formulas of the compounds that comprise the sample.

Next, a polarization correction must be made as well. Commercial x-ray tubes produce completely unpolarized radiation, which in the geometry of a θ–2θ scan results in a polarization factor of (Warren, 1990) $C_p = (1 + cos^2 2\theta)/2$. However, if a monochromator used in front of the detector, the polarization factor is $C_p = (1 + cos^2 2\theta cos^2 2\theta_{mono})/2$.

Lastly there is the Lorentz factor. This factor comes about because the theoretical diffraction peak amplitude is integrated over the q space, where as the measurement is integrated by the detector surface as well as the ω rotation during the θ–2θ scan (Warren, 1990). As a result the measured diffraction intensity is the theoretical intensity multiplied by the Lorentz factor $C_L = 1/sin2\theta$ (for the lamellar diffraction). All together the measured intensity is proportional to $|F|^2 \cdot C_{abs} \cdot C_p \cdot C_L$ where F is the diffraction amplitude.

The electronic density of the unit cell can be constructed once the amplitudes of each Bragg peak have been corrected. As with all x-ray structure determinations however, the true challenge lies in the determination of phases for each Bragg peak amplitude. The centro-

symmetry of the unit cell guarantees that phases will be either $+1$ or -1. Blaurock introduced a straightforward method for phase determination of multilamellar samples based of unit cell modulation (Blaurock, 1971). In this method, the thickness of the water layer (and hence the unit cell D-spacing) is changed via humidity control of the sample in the lamellar phase. Data taken from multiple samples or humidities may be normalized using yet another method introduce by Blaurock (Blaurock, 1971). One can then overlay experimentally obtained rescaled structure factors from different humidities, and the phases may be determined accordingly from the set that most accurately traces out the structure factor curve.

This method assumes that the overall structure of the unit cell (particularly the bilayer) remains unchanged aside from thickening/thinning the water layers at different relative humidities (Torbet & Wilkins, 1976). Discrete Fourier inversion, with the proper choice of phases, can produce electron density profiles of the unit cell. The extrapolated the bilayer thickness at full hydration is measured as the distance between the two reconstructed phosphate peaks, or the PtP distance. The observed dependence of the PtP distance on D-spacing (and hence humidity) is non-linear monotonic decreasing and approaches an asymptotic value as the D-spacing increases. This asymptotic value is taken as the bilayer thickness at full hydration.

The one-dimensional electron density profiles of the lamellar phase recovered from diffraction experiments have a characteristic shape and carry useful qualitative information beyond the numerical measurement of the PtP distance. In particular, the acyl chain region of the bilayer undergoes disorder changes as relative humidity changes. At lower relative humidities, finer features can be seen in the acyl chain region as the chains have greater correlated order in packing and tilt angles. By contrast, the acyl chain regions at higher relative humidities are much smoother, indicating more disorder in packing and tilt angles. Qualitatively, these changes may be taken as evidence that the multilayer is swelling properly with hydration, though some agents, such as cholesterol or ergosterol, can modify this general behavior when incorporated into the samples (Hung et al., 2007; Hung et al., 2016).

S2.5 Neutron in-plane scattering: detecting and sizing transmembrane pores, see (Ding et al., 2004; He et al., 1996; Huang & Yang, 2009; Yang et al., 1998).

S2.6 Multiwavelength anomalous diffraction: lipidic structure of the pores, see (Huang, 2012; Qian et al., 2008; Wang et al., 2006; Yang & Huang, 2003).

Movie S1

The movie of Figure 2. (The red line on the micropipette is an optical artifact.) At the beginning, the GUV of DOPC/DOPG 7:3 is seen by the red color of the soluble dye TRsc (MW 625, 10 μM) inside the GUV. The appearance of green on the surface of GUV indicates the binding of FITC-melittin (2 μM) outside the GUV. The binding causes the area expansion hence the protrusion in the micropipette increases. Then the intensity of red color suddenly begins to decrease and diminish, indicating the formation of stable pores in the membrane. For a while the protrusion length continued to increase due to further binding of melittin. As explained in the

section **S2.1,** the formation of stable pores causes the GUV to swell, because of our initial preparation with sucrose inside versus glucose outside the GUV. After the melittin binding reaches equilibrium the protrusion length eventually decreases due to the GUV volume increase. The real time of the movie is 400s total. Photobleaching was negligible. (Lee et al., 2013)

References

BAZZI, M. D. & WOODY, R. W. (1987). Interaction of Amphipathic Polypeptides with Phospholipids - Characterization of Conformations and the Cd of Oriented Beta-Sheets. Biopolymers, 26(7), 1115-1124.

BECHINGER, B., KIM, Y., CHIRLIAN, L. E., GESELL, J., NEUMANN, J. M., MONTAL, M., TOMICH, J., ZASLOFF, M. & OPELLA, S. J. (1991). Orientations of amphipathic helical peptides in membrane bilayers determined by solid-state NMR spectroscopy. J Biomol NMR, 1(2), 167-173.

BLAUROCK, A. E. (1971). Structure of the nerve myelin membrane: proof of the low-resolution profile. J Mol Biol, 56(1), 35-52.

BURCK, J., ROTH, S., WADHWANI, P., AFONIN, S., KANITHASEN, N., STRANDBERG, E. & ULRICH, A. S. (2008). Conformation and membrane orientation of amphiphilic helical peptides by OCD. Biophys J, 95, 3872-3881.

DING, L., LIU, W., WANG, W., GLINKA, C. J., WORCESTER, D. L., YANG, L. & HUANG, H. W. (2004). Diffraction techniques for nonlamellar phases of phospholipids. Langmuir, 20(21), 9262-9269.

DING, L., YANG, L., WEISS, T. M., WARING, A. J., LEHRER, R. I. & HUANG, H. W. (2003). Interaction of antimicrobial peptides with lipopolysaccharides. Biochemistry, 42(42), 12251-12259.

FAUST, J. E., YANG, P. Y. & HUANG, H. W. (2017). Action of antimicrobial peptides on bacterial and lipid membranes: a direct comparison. Biophys J, 112, 1-10.

FUERTES, G., GARCIA-SAEZ, A. J., ESTEBAN-MARTIN, S., GIMENEZ, D., SANCHEZ-MUNOZ, O. L., SCHWILLE, P. & SALGADO, J. (2010). Pores formed by baxalpha5 relax to a smaller size and keep at equilibrium. Biophys J, 99(9), 2917-2925.

GLASER, R. W., SACHSE, C., DURR, U. H., WADHWANI, P. & ULRICH, A. S. (2004). Orientation of the antimicrobial peptide PGLa in lipid membranes determined from 19F-NMR dipolar couplings of 4-CF3-phenylglycine labels. J Magn Reson, 168(1), 153-163.

HE, K., LUDTKE, S. J., WORCESTER, D. L. & HUANG, H. W. (1996). Neutron scattering in the plane of membranes: structure of alamethicin pores. Biophys J, 70(6), 2659-2666.

HELLER, W. T., WARING, A. J., LEHRER, R. I. & HUANG, H. W. (1998). Multiple states of beta-sheet peptide protegrin in lipid bilayers. Biochemistry, 37(49), 17331-17338.

HEMMERLE, A., MALAQUIN, L., CHARITAT, T., LECUYER, S., FRAGNETO, G. & DAILLANT, J. (2012). Controlling interactions in supported bilayers from weak electrostatic repulsion to high osmotic pressure. Proc Natl Acad Sci U S A, 109(49), 19938-19942.

HUANG, H. W. (2012). Diffraction Methods for Studying Transmembrane Pore Formation and Membrane Fusion. In Encyclopedia of Biophysics (ed. G. Roberts), pp. 460- 472 Berlin Heidelberg: Springer-Verlag

HUANG, H. W. & OLAH, G. A. (1987). Uniformly oriented gramicidin channels embedded in thick monodomain lecithin multilayers. Biophys J, 51(6), 989-992.

HUANG, H. W. & WU, Y. (1991). Lipid-alamethicin interactions influence alamethicin orientation. Biophys J, 60, 1079-1087.

HUANG, H. W. & YANG, L. (2009). X-ray methods for investigation of structures of lipid assemblies. In Handbook of Molecular Biophysics (ed. H. G. Bohr), pp. 457-502. Weinheim, Germany: Wiley-VCH Verlag GmbH & Co.

HUNG, W. C., LEE, M. T., CHEN, F. Y. & HUANG, H. W. (2007). The condensing effect of cholesterol in lipid bilayers. Biophys J, 92(11), 3960-3967.

HUNG, W. C., LEE, M. T., CHUNG, H., SUN, Y. T., CHEN, H., CHARRON, N. E. & HUANG, H. W. (2016). Comparative Study of the Condensing Effects of Ergosterol and Cholesterol. Biophys J, 110(9), 2026-2033.

KUMAR, S., ed. (2001). Liquid Crystals: Cambridge University Press.

KWOK, R. & EVANS, E. (1981). Thermoelasticity of large lecithin bilayer vesicles. Biophys J, 35(3), 637-652.

LEE, C. C., SUN, Y., QIAN, S. & HUANG, H. W. (2011). Transmembrane pores formed by human antimicrobial peptide LL-37. Biophys J, 100(7), 1688-1696.
LEE, M. T., HUNG, W. C., CHEN, F. Y. & HUANG, H. W. (2008). Mechanism and kinetics of pore formation in membranes by water-soluble amphipathic peptides. Proc Natl Acad Sci U S A, 105(13), 5087-5092.
LEE, M. T., SUN, T. L., HUNG, W. C. & HUANG, H. W. (2013). Process of inducing pores in membranes by melittin. Proc Natl Acad Sci U S A, 110(35), 14243-14248.
LEVINE, Y. K. & WILKINS, M. H. (1971). Structures of oriented lipid bilayers. Nature New Biology, 230, 69-72.
LONGO, M. L., WARING, A. J., GORDON, L. M. & HAMMER, D. A. (1998). Area expansion and permeation of phospholipid membrane bilayer by influenza fusion peptides and melittin. Langmuir, 14, 2385-2395.
LONGO, M. L., WARING, A. J. & HAMMER, D. A. (1997). Interaction of the influenza hemagglutinin fusion peptide with lipid bilayers: area expansion and permeation. Biophys J, 73(3), 1430-1439.
LUDTKE, S., HE, K. & HUANG, H. (1995). Membrane thinning caused by magainin 2. Biochemistry, 34(51), 16764-16769.
LUDTKE, S. J., HE, K., WU, Y. & HUANG, H. W. (1994). Cooperative membrane insertion of magainin correlated with its cytolytic activity. Biochim Biophys Acta, 1190(1), 181-184.
MARTIN, O. C. & PAGANO, R. E. (1987). Transbilayer movement of fluorescent analogs of phosphatidylserine and phosphatidylethanolamine at the plasma membrane of cultured cells. Evidence for a protein-mediated and ATP-dependent process(es). J Biol Chem, 262(12), 5890-5898.
MOFFITT, W. (1956). Optical Rotatory Dispersion of Helical Polymers. Journal of Chemical Physics, 25(3), 467-478.
OLAH, G. A. & HUANG, H. W. (1988a). Circular-Dichroism of Oriented Alpha-Helices .2. Electric-Field Oriented Polypeptides. Journal of Chemical Physics, 89(11), 6956-6962.
OLAH, G. A. & HUANG, H. W. (1988b). Circular dichroism of oriented α-helices. J. Chem. Phys., 89, 2531-2538.
OLAH, G. A., HUANG, H. W., LIU, W. H. & WU, Y. L. (1991). Location of ion-binding sites in the gramicidin channel by X-ray diffraction. J Mol Biol, 218(4), 847-858.
POWERS, L. & PERSHAN, P. S. (1977). Monodomain samples of dipalmitoyl phosphatidylcholine with varying concentrations of water and other ingredients. Biophys J, 20(2), 137-152.
QIAN, S., WANG, W., YANG, L. & HUANG, H. W. (2008). Structure of the alamethicin pore reconstructed by X-ray diffraction analysis. Biophys J, 94, 3512-3522.
RODRIGUEZ, N., HEUVINGH, J., PINCET, F. & CRIBIER, S. (2005). Indirect evidence of submicroscopic pores in giant unilamellar [correction of unilamelar] vesicles. Biochim Biophys Acta, 1724(3), 281-287.
ROTHSCHILD, K. J., SANCHES, R., HSIAO, T. L. & CLARK, N. A. (1980). A spectroscopic study of rhodopsin alpha-helix orientation. Biophys J, 31(1), 53-64.
SEIGNEURET, M. & DEVAUX, P. F. (1984). ATP-dependent asymmetric distribution of spin-labeled phospholipids in the erythrocyte membrane: relation to shape changes. Proc Natl Acad Sci U S A, 81(12), 3751-3755.
SUN, Y., HUNG, W. C., CHEN, F. Y., LEE, C. C. & HUANG, H. W. (2009). Interaction of tea catechin (-)-epigallocatechin gallate with lipid bilayers. Biophys J, 96(3), 1026-1035.
SUN, Y., SUN, T. L. & HUANG, H. W. (2016). Mode of Action of Antimicrobial Peptides on E. coli Spheroplasts. Biophys J, 111(1), 132-139.
TAMBA, Y., ARIYAMA, H., LEVADNY, V. & YAMAZAKI, M. (2010). Kinetic pathway of antimicrobial peptide magainin2 induced pore formation in lipid membranes. J. Phys. Chem. B, 114, 12018-12026.

TAMBA, Y. & YAMAZAKI, M. (2005). Single giant unilamellar vesicle method reveals effect of antimicrobial peptide magainin 2 on membrane permeability. Biochemistry, 44(48), 15823-15833.
TAMM, L. K. & TATULIAN, S. A. (1997). Infrared spectroscopy of proteins and peptides in lipid bilayers. Q Rev Biophys, 30(4), 365-429.
TINOCO, I., JR. (1964). Circular dichroism and rotatory dispersion curves of helices. J. Am. Chem. Soc., 86, 297-298.
TORBET, J. & WILKINS, M. H. (1976). X-ray diffraction studies of lecithin bilayers. J Theor Biol, 62(2), 447-458.
VELLUZ, L., LEGRAND, M. & GROSJEAN, M. (1965). Optical circular dichroism. New York: Academic Press.
WANG, W., PAN, D., SONG, Y., LIU, W., YANG, L. & HUANG, H. (2006). Method of x-ray anomalous diffraction for lipid structures. Biophys J, 91, 736-743.
WARREN, B. E. (1990). X-ray Diffraction. Mineola, N.Y.; pp. 41-47, 51-54.: Dover Publications,.
WEISS, T. M., VAN DER WEL, P. C., KILLIAN, J. A., KOEPPE, R. E., 2ND & HUANG, H. W. (2003). Hydrophobic mismatch between helices and lipid bilayers. Biophys J, 84(1), 379-385.
WEISS, T. M., YANG, L., DING, L., WARING, A. J., LEHRER, R. I. & HUANG, H. W. (2002). Two states of cyclic antimicrobial peptide RTD-1 in lipid bilayers. Biochemistry, 41(31), 10070-10076.
WOODY, R. W. (1985). Circular dichroism of peptides. In The Peptides eds. S. Udenfriend and J. Meienhofler), pp. 15-114. New York: Academic Press.
WOODY, R. W. (1993). The circular dichroism of oriented beta sheets: theoretical predictions. Tetrahedron Asymmetry, 4, 529-544.
WU, Y., HUANG, H. W. & OLAH, G. A. (1990). Method of oriented circular dichroism. Biophys J, 57, 797-806.
YAMAOKA, K., UEDA, K. & KOSAKO, I. (1986). Far-Ultraviolet Electric Linear Dichroism .3. Far-Ultraviolet Electric Linear Dichroism of Poly(Gamma-Methyl L-Glutatmate) in Hexafluoro-2-Propanol and the Peptide Band in the 187-250-Nm Wavelength Region. Journal of the American Chemical Society, 108(15), 4619-4625.
YANG, L., HARROUN, T. A., HELLER, W. T., WEISS, T. M. & HUANG, H. W. (1998). Neutron off-plane scattering of aligned membranes. I. Method Of measurement. Biophys J, 75(2), 641-645.
YANG, L., HARROUN, T. A., WEISS, T. M., DING, L. & HUANG, H. W. (2001). Barrel-stave model or toroidal model? a case study on melittin pores. Biophys J, 81, 1475-1485.
YANG, L. & HUANG, H. W. (2003). A rhombohedral phase of lipid containing a membrane fusion intermediate structure. Biophys J, 84(3), 1808-1817.